Five-year climatology and composite study of precipitation bands associated with extratropical cyclones over the British Isles

DOI:
10.1175/WAF-D-22-0207.1

Document Version
Accepted author manuscript

Citation for published version (APA):
Zhang, T., & Schultz, D. (2023). Five-year climatology and composite study of precipitation bands associated with extratropical cyclones over the British Isles. *Weather and Forecasting*. https://doi.org/10.1175/WAF-D-22-0207.1

Published in:
Weather and Forecasting

Five-year climatology and composite study of precipitation bands associated with extratropical cyclones over the British Isles

Tianhang Zhang[a] and David M. Schultz[a,b]

[a] *Centre for Atmospheric Science, Department of Earth and Environmental Sciences, University of Manchester, Manchester, United Kingdom*

[b] *Centre for Crisis Studies and Mitigation, University of Manchester, Manchester, United Kingdom*

For submission as an Article to *Weather and Forecasting*

21 November 2022; Revised 6 April 2023

Corresponding author: Tianhang Zhang, tianhang.zhang@postgrad.manchester.ac.uk.

ABSTRACT

A five-year climatology and composite study of precipitation bands associated with extratropical cyclones over the British Isles from April 2017 to March 2022 are constructed. A total of 249 single bands were manually identified from radar network mosaics in association with 167 cyclones identified from surface maps. More bands formed over water near the coast than over inland areas, and most had a meridional orientation. The average lengths of bands at the times of formation and maximum length were 290 and 460 km, respectively; only 20% of bands reached a maximum length exceeding 600 km. The number of bands decreased with increasing duration, with 31% of bands lasting for 2–3 h, with bands lasting more than 10 h uncommon. The bands were classified into six categories, with occluded-frontal bands (19 yr^{-1}), warm-frontal bands (11 yr^{-1}), and cold-frontal bands (10 yr^{-1}) being the most frequent. Occluded-frontal and warm-frontal bands commonly occurred west of Scotland and in the east quadrant relative to their parent cyclones. In contrast, cold-frontal bands commonly occurred southwest of Great Britain and in the south quadrant relative to their parent cyclones. Composites for northwest–southeast occluded-frontal and warm-frontal bands west of Scotland, and southwest–northeast cold-frontal bands southwest of Great Britain, show the different synoptic environments that favor bands. The low-level jet transports moisture into the band and is similar to the location and scale of the composite bands, similar to that of an atmospheric river. These results are compared to previous studies on bands from the United States.

SIGNIFICANCE STATEMENT

Precipitation bands are lines of heavy precipitation as seen on weather radar. Most studies of bands in extratropical cyclones have occurred in the United States. We examine five years of bands in extratropical cyclones over the British Isles to better understand their characteristics. Bands form in preferred geographic regions: offshore of the west coasts of Scotland, Wales, and southwest England. The most common bands are associated with occluded fronts (37% of all bands). The average scale of the bands is associated with the average scale of wind maxima 1–2 km above ground. These results provide a better understanding of the typical characteristics and conditions under which bands form and their geographical variability compared to the United States.

1. Introduction

Extratropical cyclones produce much of the precipitation in the midlatitudes, as much as 90% of the total winter precipitation in some regions (Hawcroft et al. 2012). The heaviest precipitation within such cyclones often organizes on the mesoscale into linear or quasi-linear features called *precipitation bands* (encompassing both rainbands and snowbands). For instance, 85% of precipitation systems in northeast United States cyclones (Novak et al. 2004) and 63% of snowfall events in the central United States cyclones (Baxter and Schumacher 2017) were associated with banded precipitation. In another example, linear rainfall systems, which were often convective and associated with fronts and lows, occurred every 6–7 days over Melbourne, Australia (Hitchcock et al. 2021). Regardless of their locations, such bands can produce extreme weather such as heavy rain, flooding, or snow, which can disrupt society, causing damage, injuries, and sometimes death. Thus, better understanding of when, where, and under which conditions precipitation bands occur may lead to their improved prediction, reducing losses of property and life.

Climatologies can be helpful to better understand characteristics (e.g., location, duration, shape, size) of precipitation bands for a long period over a defined region. Although a number of climatologies have been constructed of precipitation bands associated with cyclones in the United States (e.g., Novak et al. 2004; Novak et al. 2010; Baxter and Schumacher 2017; Ganetis et al. 2018) , other regions are less likely to have their own climatologies. Specifically, no climatology exists of precipitation bands associated with cyclones over the British Isles (i.e., the United Kingdom and Ireland). Thus, we will create a climatology of precipitation bands in cyclones and their characteristics to compare between these two locations.

Another approach that has been used in the past is classification schemes of precipitation bands. The first such scheme was Houze et al. (1976), who classified precipitation bands in cyclones in the Pacific Northwest into six types by the locations relative to their fronts: warm-frontal, wide cold-frontal, narrow cold-frontal, warm-sector, wave-like, and postfrontal bands. Later incarnations of this scheme included prefrontal cold-surge bands (Hobbs 1978; Matejka et al. 1980; Houze and Hobbs 1982) and occlusion bands (Houze 2014, his Fig. 11.24). In the United

Kingdom, Browning (1986) broadly adopted the Houze scheme, although dividing the precipitation features associated with cold fronts into anafronts and katafronts, following Bergeron (1937) and Sansom (1951). Beyond that scheme, there may also be regional variability in the structure of cyclones and their precipitation bands. For example, Parsons and Hobbs (1983) showed that five Pacific cyclones all had cold-frontal bands, but no warm-frontal bands. In contrast, most bands in northeast U.S. cyclones were associated with the vertical extension of the surface warm front or surface occluded front (Novak et al. 2004). Therefore, a question arises as to what types of bands dominate over the British Isles. We will create a climatology of band types based on the classification scheme in the present study to address this question, which helps further understand which fronts are responsible for producing precipitation bands over the British Isles.

Moisture, lift, and instability are three ingredients for producing heavy precipitation. Low-level jets are often present in association with banded precipitation, providing both dynamical and thermodynamical support for the bands. For example, low-level jets contribute to the formation and maintenance of bands through both moisture transport and ascent at their leading edges (e.g., Browning and Pardoe 1973; Ninomiya and Akiyama 1974; Lackmann 2002). Many composite and case studies have showed that frontogenesis in the presence of moist symmetric instability or small moist symmetric stability may favor the formation of precipitation bands (e.g., Emanuel 1985; Thorpe and Emanuel 1985; Sanders 1986; Xu 1989, 1992; Nicosia and Grumm 1999; Novak et al. 2004; Moore et al. 2005; Novak et al. 2008; Kawashima 2016). In contrast, other studies have suggested that moist symmetric instability is not a necessary feature during the formation of precipitation bands in extratropical cyclones (e.g., Schultz and Schumacher 1999; Novak et al. 2010). Regardless, how these ingredients come together to produce the observed panoply of bands over the British Isles remains an active area of research. In this study, composite analyses are created for studying common synoptic environments of various types of bands.

Specifically, the aim of this study is to establish a five-year climatology of precipitation bands over the British Isles from April 2017 to March 2022. To better understand their features, the following questions will be addressed in this study:

- Where do precipitation bands frequently occur?

- What types of bands are present?
- What are the characteristics of different types of bands (e.g., frequency, duration, geographical, surface cyclone–relative distribution)?
- What are the synoptic environments that favor the common types of bands?

The structure of this article is as follows. Section 2 introduces the data and methods used to construct the five-year climatology. Section 3 shows the geographical locations of extratropical cyclones and precipitation bands, whereas section 4 presents the lengths and durations of precipitation bands. Section 5 discusses a classification scheme of bands according to the location relative to their fronts. Section 6 provides composite analyses of synoptic environments for occluded-, warm-, and cold-frontal bands. Finally, section 7 concludes this article.

2. Data and methods

To create a climatology of precipitation bands associated with extratropical cyclones over the British Isles, two datasets are required: a dataset of cyclones and a radar-based dataset of precipitation rates.

First, a dataset was established for cyclones from April 2017 to March 2022. This period was selected because many radar data in the archive (introduced in the next paragraph) were absent before April 2017 and the present study commenced after March 2022. The Deutscher Wetterdienst (DWD, German Weather Service) surface-map analysis archive (http://www1.wetter3.de/) was used to develop a database of surface cyclones over the eastern North Atlantic Ocean and Europe. The maps were available at 0000, 0600, 1200, and 1800 UTC. A cyclone was defined as at least one closed isobar (5-hPa contour intervals on the DWD maps) with a minimum central pressure less than 1000 hPa within the domain (40–70°N, 40°W–20°E) and possessing fronts that were across the radar-data domain (defined in the next paragraph). The cyclone needed to have been present for at least 24 h (or five consecutive map times), following the approaches of Gulev et al. (2001) and Ganetis et al. (2018). The minimum central-pressure and duration criteria were employed to remove cyclones that were weak and short lived. The result of this analysis was a dataset of 554 cyclones.

Second, having constructed a dataset of 554 potential parent cyclones, precipitation bands associated with these cyclones were identified from 30-min archived radar imagery from the commercial Metcheck website (https://www.metcheck.com/WEATHER/archived_radar.asp). Electromagnetic pulses are emitted by radars from the networks of the United Kingdom's Met Office and the Republic of Ireland's Met Éirrean and scattered by precipitation droplets at non-zero elevation angles (typically between 0.5° and 4°). Imagery is derived from a mosaic analysis of radar reflectivity interpolated to 1 km above sea level converted into rainfall rate. Further details of the network, data processing, and mosaic can be found in Kitchen and Illingworth (2011), Antonescu et al. (2013), and Fairman et al. (2017). The radar domain covers the British Isles (48°–60°N, 12°W–4°E) and is smaller than the cyclone domain. This difference in domain sizes in the present study is because a cyclone center may be located outside of the radar domain, but fronts associated with this cyclone may be located within the radar domain and produce precipitation bands. When there were multiple surface lows occurring at the same time in one cyclone, the low center whose fronts were closest to the band was used.

In this study, we do not discriminate between rainbands and snowbands, although it is likely that nearly all the bands were associated with rain at the surface at low-elevation stations. We only focus on single (i.e., one linear feature) precipitation bands and manually identify bands that meet the following criteria:

- a contiguously linear or quasi-linear feature,
- an intensity of at least 2 mm h^{-1} (28 dBZ) for at least 200 km length,
- an aspect ratio (the ratio of length to width) of 3:1 or greater, and
- a duration of at least 2 h.

These criteria are similar to those used by Novak et al. (2004), Baxter and Schumacher (2017), and Ganetis et al. (2018). Length and width (i.e., of the widest part) here are defined as the distance along the maximum and minimum axes of a region with 2 mm h^{-1} rainfall, respectively (Fairman et al. 2016). The duration is defined as the length of time over which a band met all the above-mentioned criteria over the radar domain. The minimum separation in time for one band to end and a new one to be considered is at least one hour. The "formation" time is the time when a band formed (i.e., first met the above criteria). Naturally, bands meeting these criteria did not suddenly appear at this time (hence the quotes around "formation"), but some precursor features (i.e., precipitation that does not meet our criteria for banding) will likely be present for tens of minutes, or even hours perhaps, before meeting our criteria for band formation. In this study, we apply a manual band identification approach rather than an automated approach (as in Fairman et al. 2017). We chose a manual approach because of the large amount of work of constructing an automated approach that matched precipitation bands from radar data to extratropical cyclones from a separate database. Consequently, the ease of identifying precipitation bands manually from online image archives of radar and surface maps surpassed the effort of constructing an automated approach using digital radar data and cyclone tracks from reanalyses.

In this study, a small number of bands (22 out of 249 bands) extended beyond the radar domain. For those cases, we just considered their parts within the domain. The distance between a band and its associated front, if any, needed to be less 350 km. The purpose of setting this threshold was to remove bands that had distant relationships, if any, to fronts. After these criteria were applied, a total of 249 bands associated with 167 cyclones occurred over the British Isles. Over the 5-yr period from April 2017 to March 2022, there was an annual average of 50 bands and 219 h of bands (Table 1). Despite some interannual variability (Table 1), these quantities and others not shown exhibited consistency from year to year, demonstrating that five years was sufficient to capture the salient features of these bands and their characteristics.

Table 1. Annual number and time of precipitation bands from April 2017 to March 2022 over the British Isles.

Year	Apr 2017–Mar 2018	Apr 2018–Mar 2019	Apr 2019–Mar 2020	Apr 2020–Mar 2021	Apr 2021–Mar 2022	Average
Number	49	41	48	53	58	50
Time (h)	217	181.5	241	216	238.5	219

Third, we define types of bands by the nearby front, if any, at the formation time. To classify bands by their positions relative to fronts, we need to compare DWD surface maps and radar imagery from the Metcheck archive at the same time. However, the interval between DWD surface maps (6 h) is longer than the interval between successive radar images in this archive (30 mins), meaning that it is not possible to match each radar image to a DWD surface map. Thus, if the band were present between two map times, the closest 6-h map time before or after the formation time is chosen. If the band forms in the middle of two map times, the average location of cyclones and fronts is used. Next, we placed surface maps of all cases with the radar images overlaid or side-by-side to see where the projected position of the front from the DWD image was relative to the band on the Metcheck archive. For most bands, the position of a band relative to the front was clear.

The most popular classification scheme of precipitation bands is that from Houze (2014, chapter 11 and his Fig. 11.24). However, the classification scheme in the present study is a little different from that in Houze (2014). First, because we do not involve upper-air maps in our method, we do not have the ability to distinguish the upper-level cold front and prefrontal surge bands. Thus, we classify bands only based on the surface fronts. Second, we do not discriminate between Houze's (2014) narrow cold-frontal bands and wide cold-frontal bands, and instead refer to both as cold-frontal bands. Therefore, we classify six types of bands as follows (Fig. 1):

- *Occluded-frontal bands* occur along or ahead of an occluded front.
- *Cold-frontal bands* occur parallel to and along the cold front or a little behind the cold front (in the direction of motion of the front).
- *Warm-frontal bands* occur ahead of and parallel to the warm front.
- *Warm-sector bands* occur parallel to and ahead of the cold front.
- *Postfrontal bands* occur behind and parallel to the cold front or occluded front.
- *Other bands* are precipitation bands that do not meet any of the other definitions above (e.g., precipitation associated with secondary fronts, bands parallel to the warm front in the warm sector). Specifically, Doswell (1991) has advocated for having an unclassifiable category for events that do not fit into other named categories.

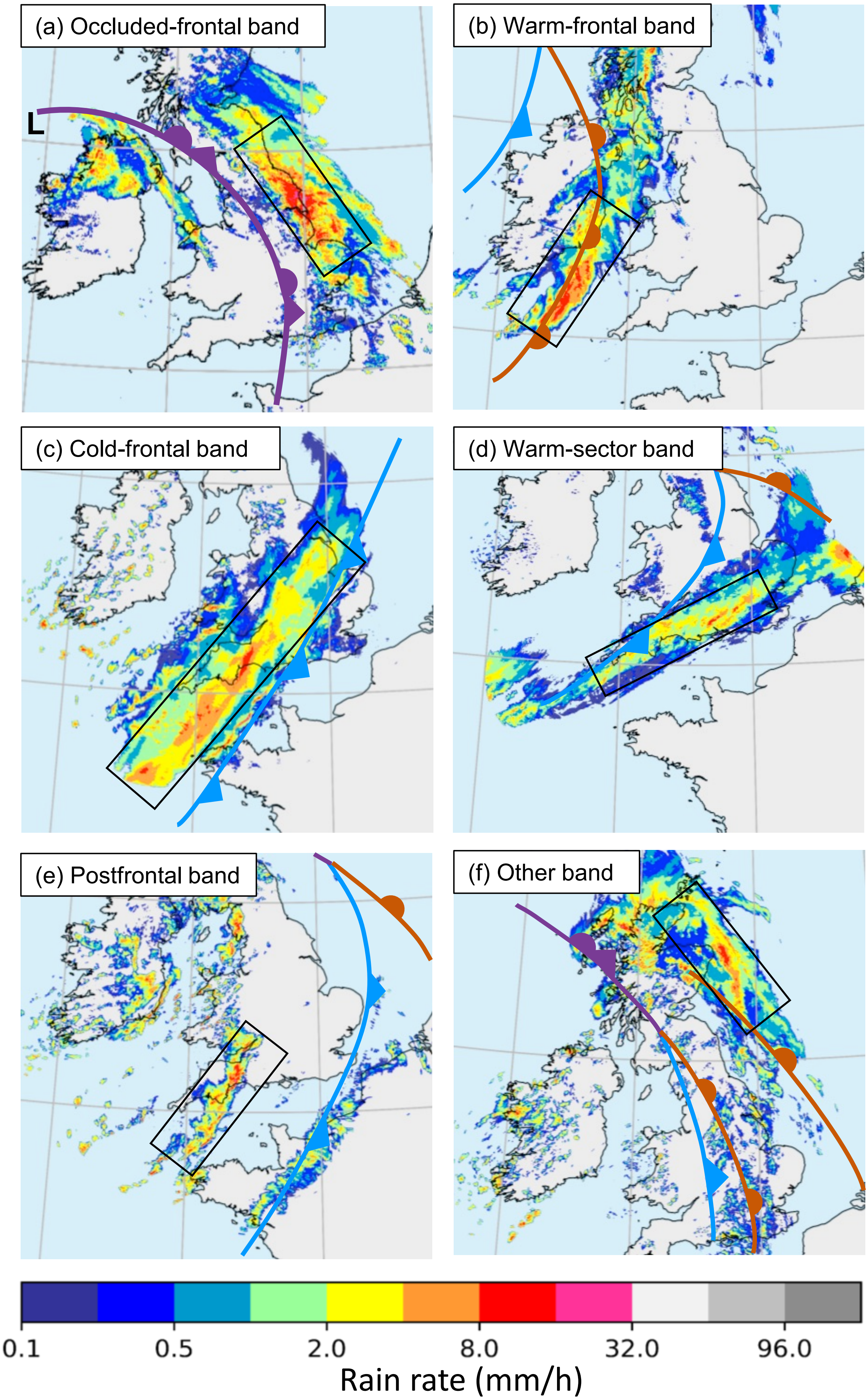
(a) Occluded-frontal band
L
(b) Warm-frontal band
(c) Cold-frontal band
(d) Warm-sector band
(e) Postfrontal band
(f) Other band
0.1
0.5
2.0
8.0
32.0
96.0
Rain rate (mm/h)

231

Figure 1. Precipitation rates (mm h^{-1}, colored according to scale) of an (a) occluded-frontal band at 0000 UTC 4 Oct 2019, (b) warm-frontal band at 0600 UTC 6 Dec 2018, (c) cold-frontal band at 1200 UTC 12 Mar 2019, (d) warm-sector band at 1200 UTC 24 Feb 2020, (e) postfrontal band at 0000 UTC 14 Dec 2020, and (f) other band at 1800 UTC 13 Dec 2020. Black boxes represent the region with a band.

3. Geographical locations of extratropical cyclones and precipitation bands

Analysis of DWD surface maps and radar images for each precipitation band from April 2017 to March 2022 was performed to better understand the geographical distributions of the extratropical cyclones (section 3a) and precipitation bands (section 3b).

a. Geographical distribution of extratropical cyclones

Figure 2 maps the distribution of 249 low-pressure centers, encompassing 167 unique extratropical cyclones associated with precipitation bands over the British Isles at their formation times. The seasonal variation in the location of the cyclone centers is small, with cyclones being found within and to the west, northwest, and north of the radar domain (Fig. 2). Cyclones approaching from the south and southwest are less common. This distribution of low centers is similar to Dacre and Gray (2009, their Figure 2a), showing a higher density of cyclones west and northwest of the British Isles; however, Dacre and Gray (2009) does not show the seasonal variation.

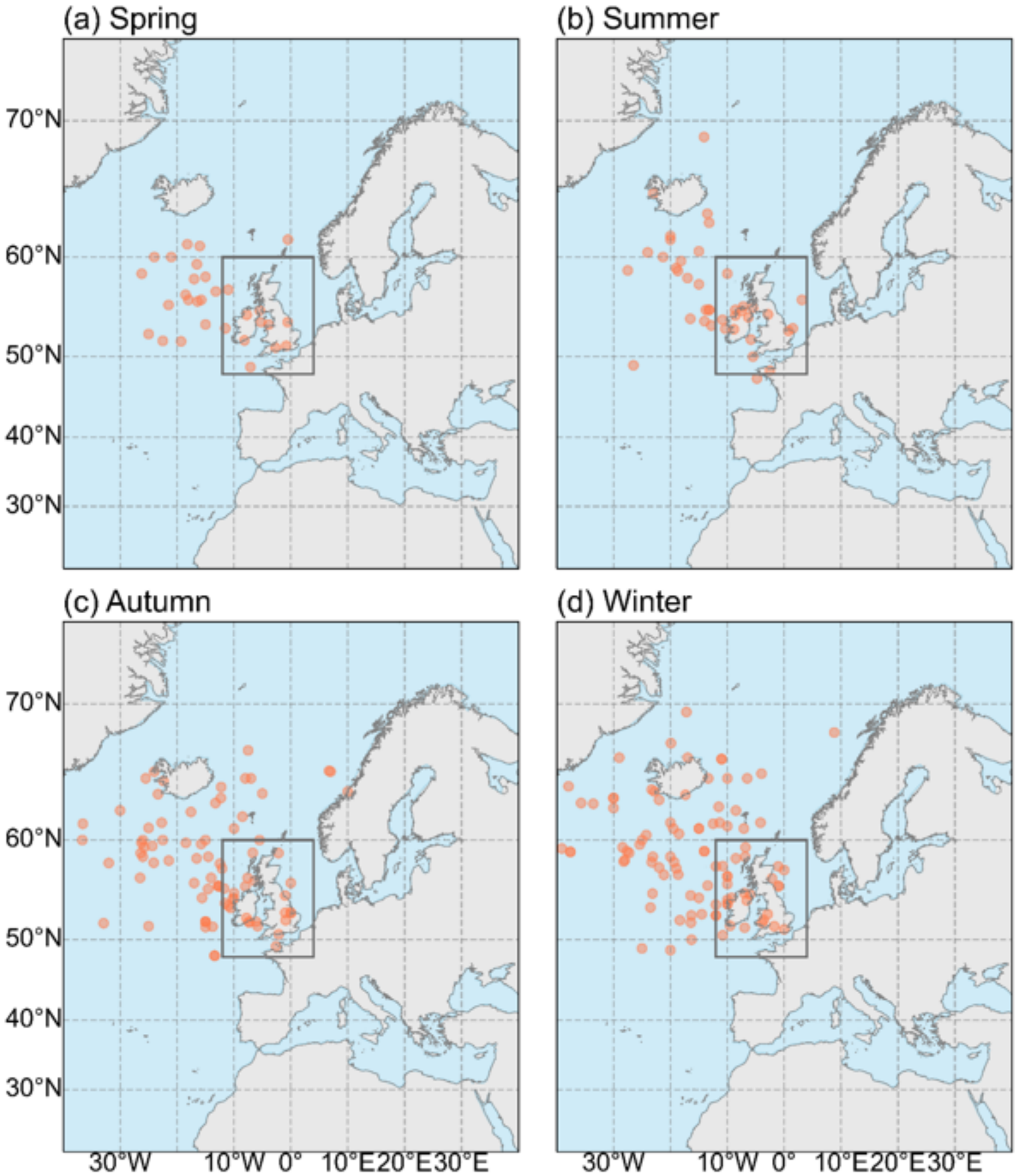

Figure 2. The locations of the 167 surface low centers corresponding to each of the 249 precipitation bands in (a) spring (MAM), (b) summer (JJA), (c) autumn (SON), and (d) winter (DJF) at the formation time of the band, where the red dot represents the position of each surface low. Gray boxes represent the radar domain described in section 2.

b. *Geographical distribution of precipitation bands*

The seasonal change in positions of precipitation band formation shows that bands are more frequent in autumn and winter than in spring and summer over the British Isles (Fig. 3), similar to Fig. 13 in Fairman et al. (2017). In winter and spring, precipitation bands are prevalent near the west coastline of Scotland (30%, or 29 of all 97 winter bands, and 27%, or 8 out of all 30 spring bands) and near the southwest coastline of Great Britain (including west of Wales and southwest of England) (23%, or 22 bands of all 97 winter bands, and 21%, or 6 bands of all 30 spring bands) (Figs. 3a,d). However, in summer and autumn, precipitation bands are prevalent west of Ireland (30%, or 12 of all 40 summer bands, and 30%, or 25 out of all 82 autumn bands) (Figs. 3b,c). Another study that examined the distribution of banded precipitation by season over the British Isles was Fairman et al. (2017), who used an automated detection scheme to identify 1,803,209 banded features from 2006 to 2015, albeit not necessarily associated with extratropical cyclones (such as isolated convective storms and elevated terrain). They also found that west of Scotland, Wales, and Northern Ireland had relatively high banded-precipitation frequency (their Fig. 13). Therefore, despite the different method to automatically detect a large number of bands by Fairman et al. (2017), the distribution of our manually detected bands in a relatively smaller-sized sample is in good qualitative agreement.

Most of the precipitation bands have a predominant meridional orientation as opposed to a more zonal orientation (Fig. 3). This predominant orientation suggests that the fronts and the bands are being stretched meridionally, consistent with cyclones being near the end of their life cycle in the diffluent exit region of the North Atlantic storm track. This result is based on observations and idealized model simulations of baroclinic waves in confluence and diffluence in previous literature (e.g., Schultz et al. 1998; Schultz and Zhang 2007). However, Novak et al. (2004) and Baxter and Schumacher (2017) have different results with their cases being primarily zonally oriented. The zonal orientation of the northwest-banded composite in Novak et al. (2004) is because they are occurring in a confluent background-flow pattern at the entrance region to the North Atlantic storm track (their Fig. 5b). In the case of their nonbanded composite in which the precipitation is associated with a zonal frontal region, the flow is also in a confluent flow pattern (their Fig. 8b). The same background-flow patterns are seen with the snowbands in Baxter and Schumacher

(2017), which is zonal and associated with a confluent flow pattern (their Figs. 8a and 9a).

Another result from Fig. 3 is that there is a slightly greater tendency for bands to form over water in the autumn (62%, 51 out of 82 bands) and winter (62%, 60 out of 97 bands) than in the spring (57%, 17 out of 30 bands) and summer (58%, 23 out of 40 bands). In general, more precipitation bands form over water near the coast than over inland areas (151 versus 98 bands). Three proposed reasons could explain why. First, some bands meeting our criteria are likely in existence outside the radar domain. When they enter the domain, they qualify to be included in the band database. Even if not classified as bands by our criteria, the closer the band gets to the land (i.e., where the radars are), the more likely the more intense parts of the band closest to the Earth are sampled by the radar. Both of these situations give the appearance of bands forming over the water. Second, upstream blocking by stable prefrontal flow trapped by onshore topography may intensify the band as much 20–100 km upstream from the coastline, as observed in other cases (e.g., Colle et al. 1999; Yu and Smull 2000; Colle et al. 2002). Third, the intensity of a frontal updraft in a landfalling cold front may increase about 20 km offshore due to increased friction onshore and convergence associated with gradients in surface friction (Muir and Reeder 2010). All three of these explanations are plausible, but, at this time, the reasons for this preponderance of cases near the coasts are not known, suggesting opportunities for future research.

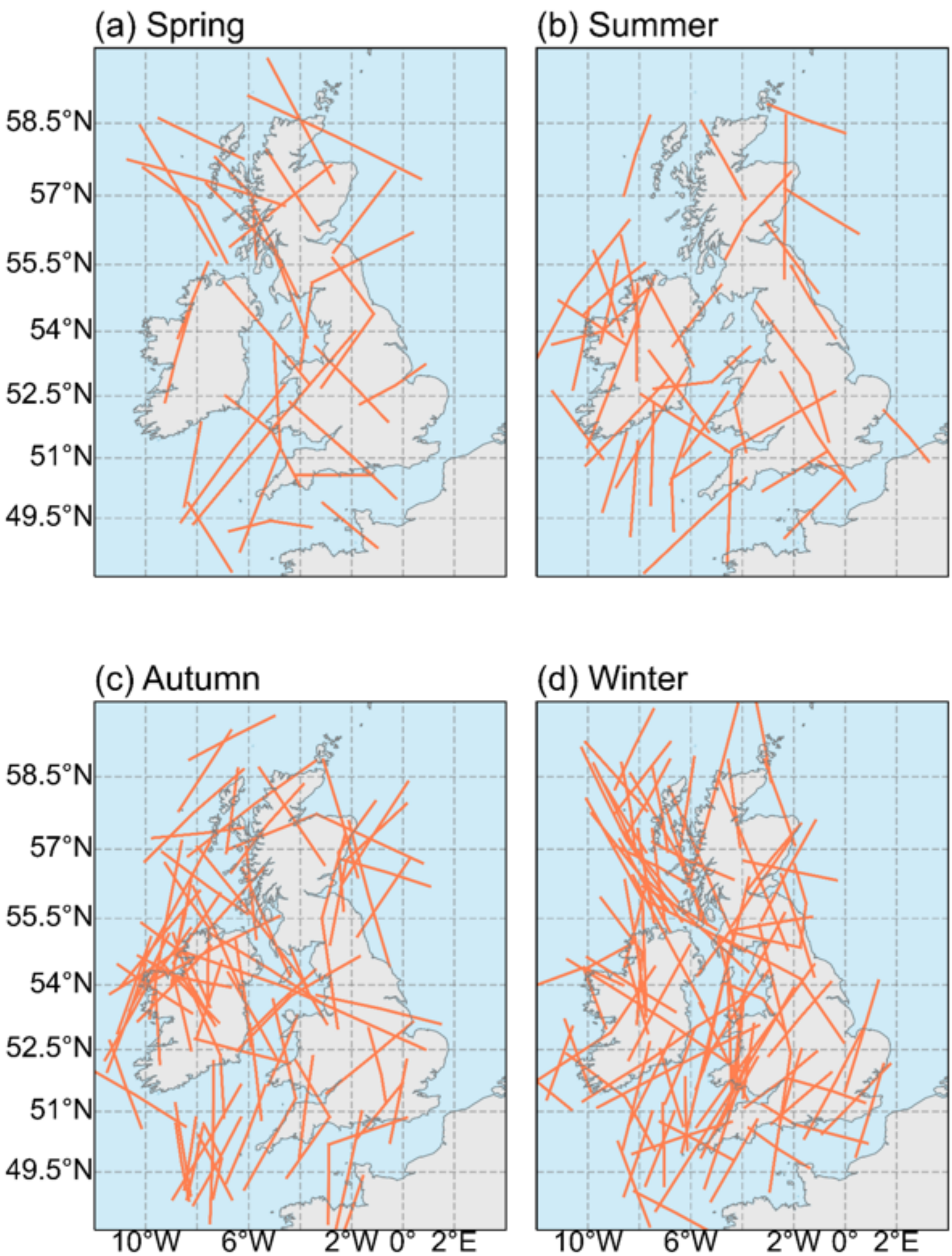

Figure 3. The geographical distribution of precipitation bands in (a) spring (MAM), (b) summer (JJA), (c) autumn (SON), and (d) winter (DJF) from April 2017 to March 2022. Red solid lines represent the bands at the formation time.

4. Characteristics of precipitation bands

In this section, characteristics of precipitation bands will be discussed. First, we compare the band length at the formation time and the maximum length (section 4a). Then, we examine how long bands lasted (section 4b).

a. Lengths of precipitation bands

The distribution in the lengths of precipitation bands is shown in Fig. 4. At the formation time of bands (which will be influenced by the minimum length to be considered a band by our criteria), 71% are 200–300 km, and the number of bands decreases with increasing length (Fig. 4a). The mode in the maximum length is 300–400 km (27%), followed by bands between 200–300, 400–500, and 500–600 km in length (17–18%) (Fig. 4b). Only 20% of bands are longer than 600 km at their maximum length. The mean maximum length of bands is 460 km, longer than the mean length at their formation time (about 290 km). This increase in the mean length of bands from their time of formation to their time of maximum length is consistent with the development of bands and is similar to the depicted growth of snowbands in Baxter and Schumacher (2017).

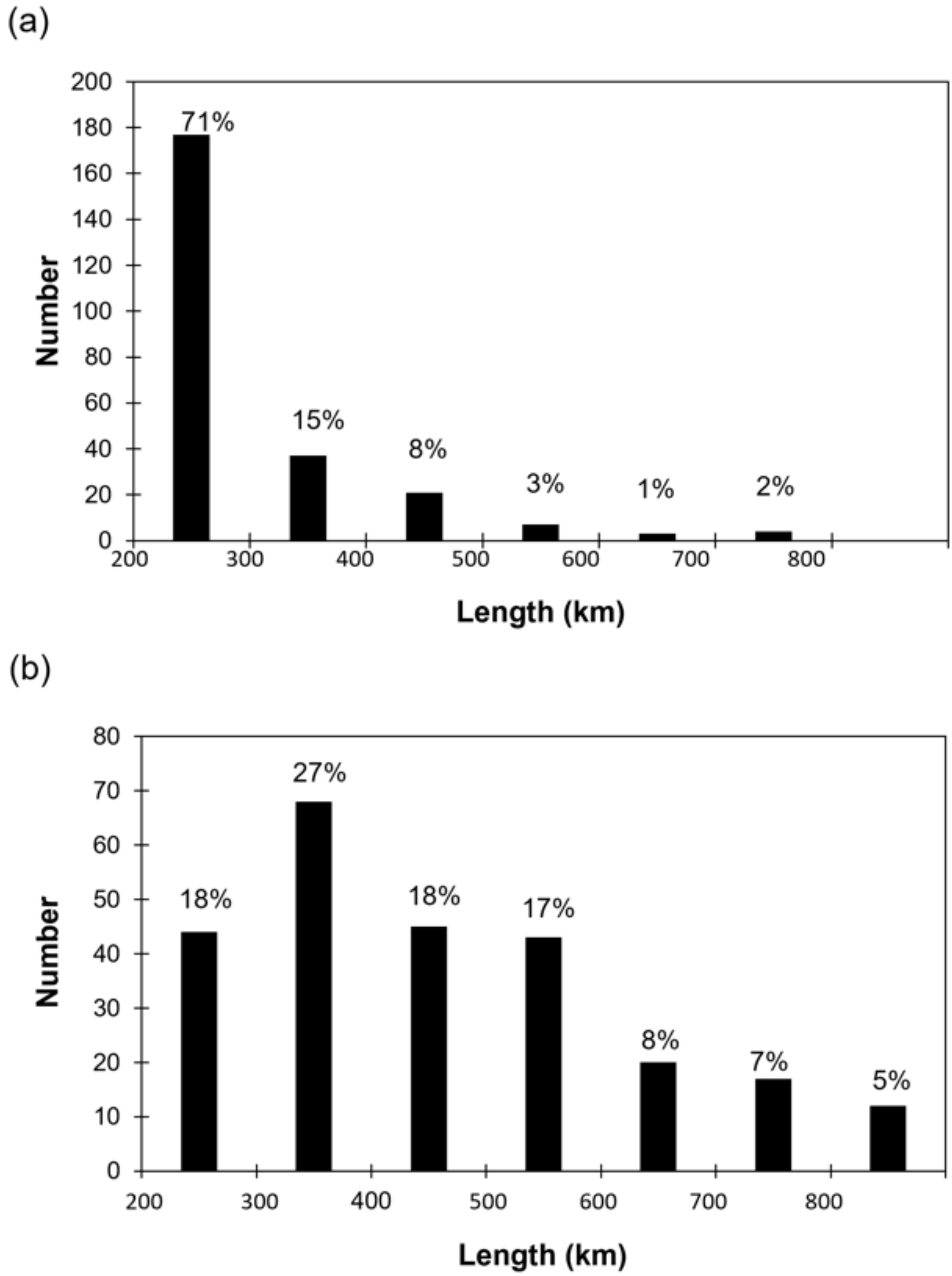

Figure 4. Distributions of the lengths of 249 precipitation bands (a) at their formation times and (b) at their maximum lengths.

b. Duration of precipitation bands

To understand the longevity of precipitation bands, a histogram of band duration is constructed (Fig. 5). Most bands are generally short-lived, with 78 bands (31%) lasting for 2–3 h, followed by 64 bands (26%) lasting 3–4 h. Bands lasting for more than 10 h are uncommon. The short duration is generally a result of the physical processes associated with the bands themselves and is not due to the bands exiting or nearing the edge of the domain. The distribution of durations for bands in Fig. 5 is consistent with that over the northeast United States in Novak et al. (2004, their Table 3) who found that the number of bands decreased with increasing band duration and most bands lasted less than 6 h and consistent with Baxter and Schumacher (2017, their Fig. 5d) who found mean values of band duration of about 5 h.

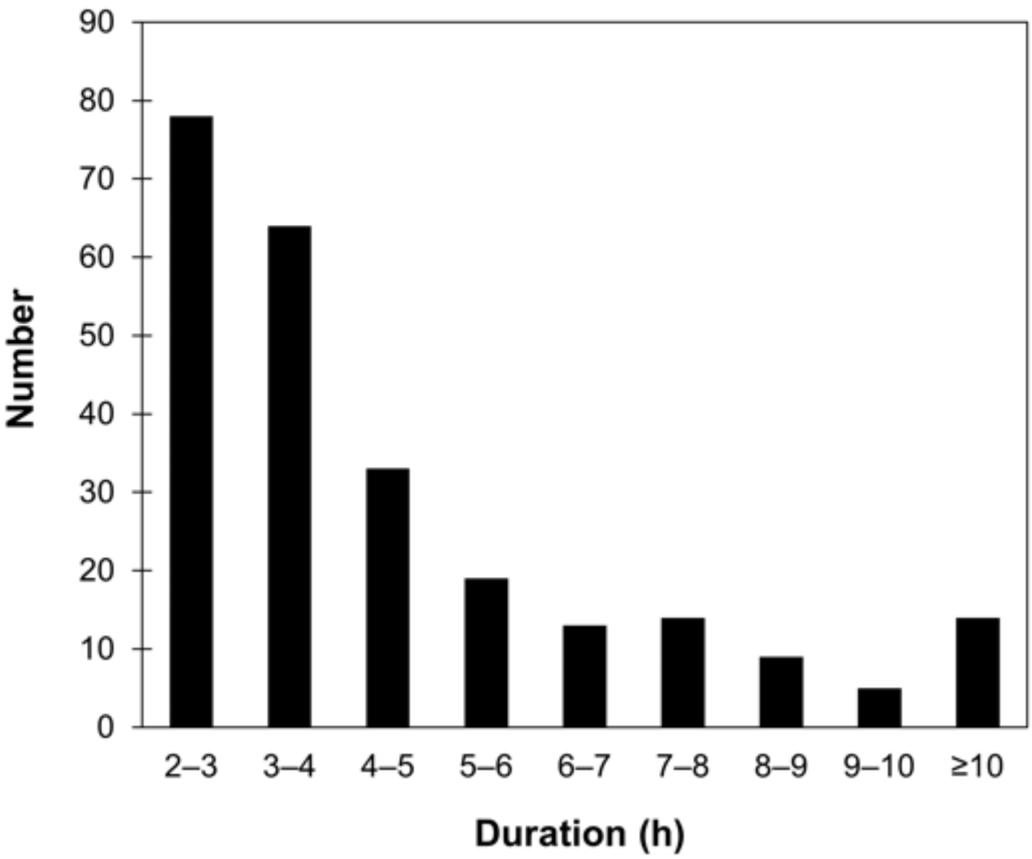

Figure 5. The duration of 249 precipitation bands from April 2017 to March 2022 ("2–3" means that the duration is at least 2 h but less than 3 h).

5. Types of precipitation bands

The classification scheme of precipitation bands in section 2 is used to establish a dataset of band types. This section further explores the classifications of bands, specifically their frequencies and durations (section 5a), and their geographical and surface cyclone–relative distributions (section 5b).

a. *Frequency and duration of the six band types*

The average number per year and average duration of various types of precipitation bands over the British Isles during the study period are shown in Fig. 6. The most frequent precipitation band type is occluded-frontal bands (19 yr^{-1}), followed by warm-frontal bands (11 yr^{-1}), cold-frontal bands (10 yr^{-1}), warm-sector bands (4 yr^{-1}), postfrontal bands (4 yr^{-1}), and other bands (3 yr^{-1}) (Fig. 6). The large number of occluded-frontal bands is consistent with observations that indicates many cyclones approaching the British Isles are late in their life cycles as opposed to early in their life cycles (e.g., Dacre and Gray 2009). The average duration is the mean number of hours of each different type of band present in radar images. In Fig. 6, the duration of all types of bands is close, fluctuating at about 4.4 h. Warm-frontal bands are the shortest-lived among these types with an average duration of 3.8 h, although they are the second most frequent. Conversely, the duration of cold-frontal band is longest (4.8 h), but their frequency is relatively small.

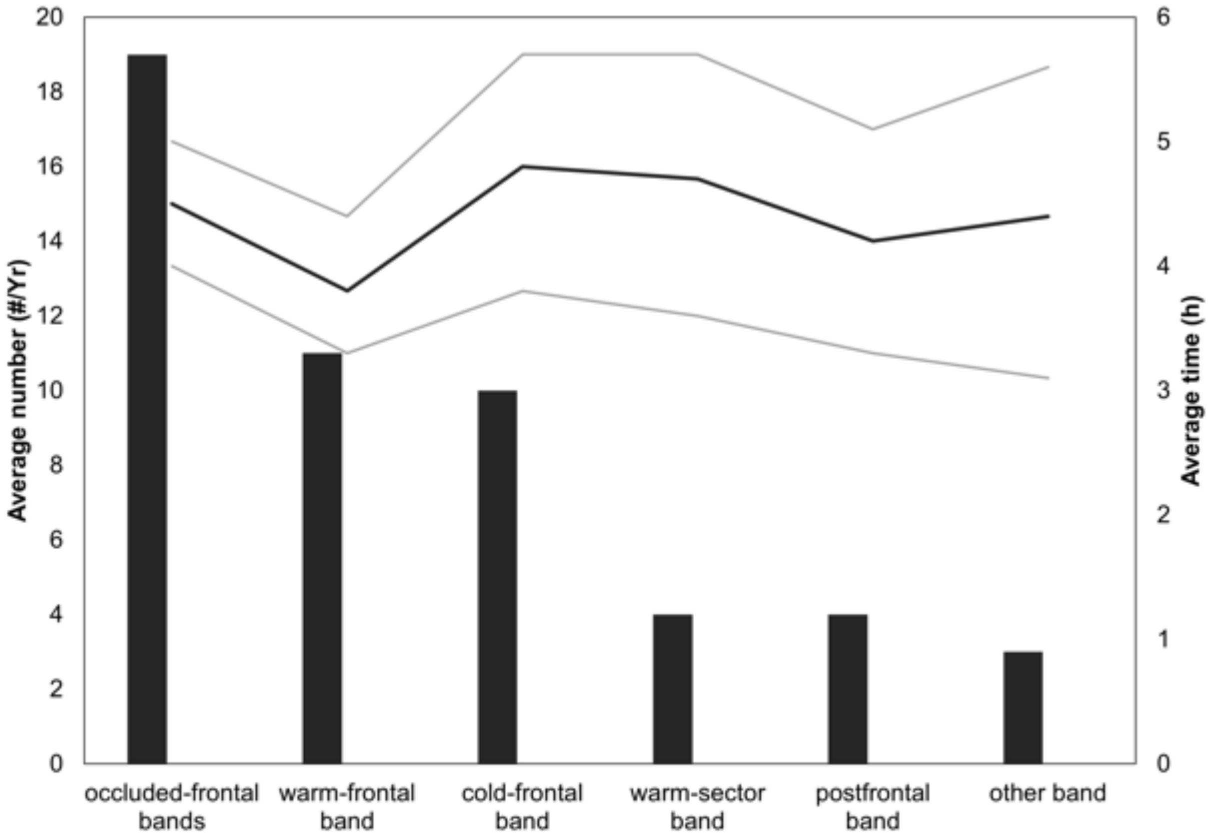

Figure 6. Average number of bands per year (bars) and average durations per band (thick black line) with 90% confidence intervals overlaid (thin gray lines) of the six types of precipitation bands from April 2017 to March 2022 over the British Isles.

b. The geographical and surface cyclone–relative distribution

This subsection discusses the geographical location of each type of precipitation band in Fig. 7 and compares it with the parent cyclone in Fig. 8. Due to the small sample sizes of warm-sector, postfrontal, and other bands, we focus on occluded-frontal, warm-frontal, and cold-frontal bands.

Figures 7a,b show occluded-frontal and warm-frontal bands are common west of Scotland (29%, or 27 out of 93 bands, and 31%, or 17 out of 54 cases, respectively). In this region, most are oriented northwest–southeast (19 occluded- and 14 warm-frontal bands). In contrast, only a few cold-frontal bands form in this region. Instead, the common location for cold-frontal bands (44%, or 21 out of 48 cases) is near the southwest coastline of Great Britain, with 90% bands (19 of those 21 cases) oriented southwest–northeast (Fig. 7c).

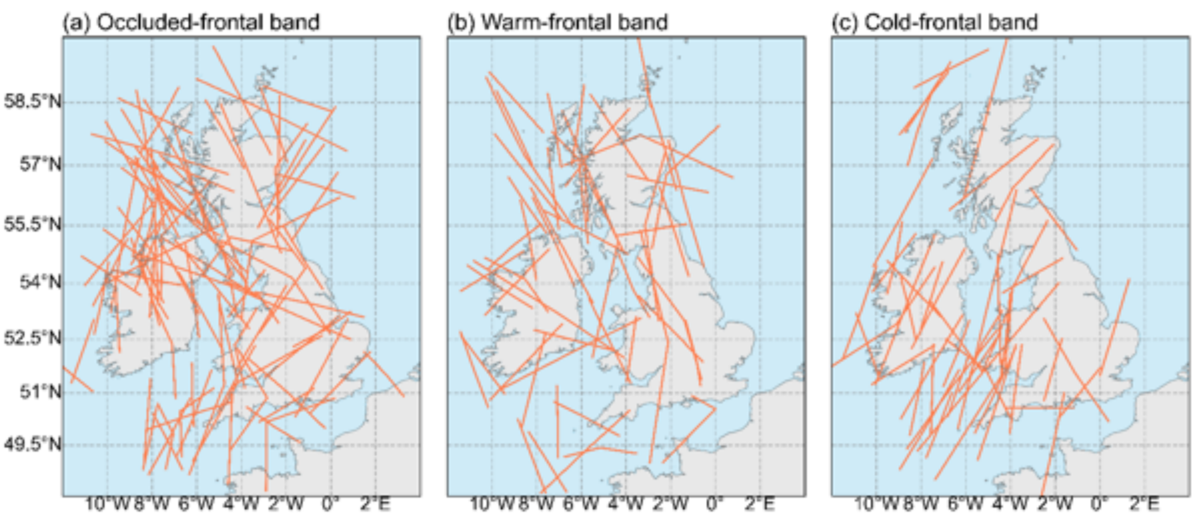

Figure 7. The geographical distribution of (a) occluded-frontal bands; (b) warm-frontal bands; (c) cold-frontal bands from April 2017 to March 2022. Red solid lines represent bands at their formation times.

Examining just the 93 occluded-frontal bands (Fig. 8a), 61% (57) of the occluded-frontal bands are totally or partially in the east quadrant (45°–135°). Most (84%, or 48) bands in this quadrant are oriented from northwest to southeast, whereas southwest–northeast bands are prevalent in other quadrants, occupying 75% (27 of 36). Similar to occluded-frontal bands, up to 78% (42 of 54) warm-frontal bands occur in the east quadrant, and their orientations tend to be northwest–southeast (Fig. 8b). Cold-frontal bands have a different distribution, where 71% (34 of 48) are in the south quadrant (135°–225°), and no band is located north of the surface low (Fig. 8c). Almost all (88%, or 42) cold-frontal bands are oriented south-southwest–north-northeast, which as mentioned before is consistent with the fronts being meridionally stretched in the diffluent exit region of the North Atlantic storm track (e.g., Schultz et al. 1998; Schultz and Zhang 2007). In general, 57% (143 of 249) bands are located in the east quadrant of cyclones, followed by 29% (73 of 249) bands in the south quadrant, likely because most cyclones are located west of the British Isles at the band-formation time (Fig. 2).

The surface cyclone–relative locations of bands in the present study differ from those shown in Novak et al. (2004) and Ganetis et al. (2018) (where the most bands occurred in the northwest quadrant over the northeast United States) and Baxter and Schumacher (2017) (where most bands were in the northeast quadrant over the central United States). This result is likely because, in the present study, the radar network is located to the east of where the cyclones are, leading to a preference for observing bands on the east side of cyclones. In contrast, for cases in the northeast United States, the radars are located on land, and thus the west side of the cyclone tracks is likely to be better observed within the radar network. However, these differences in the positions of the radar networks do not preclude the possibility that geographical differences in where bands and cyclones happen may also help to explain these differences. Second, the northeast and central United Status are at the start-of-the-storm track, different from the British Isles at the end-of-the-storm track. There may be potential physical reasons that affect the surface cyclone–relative locations of bands, beyond the scope of this study. Finally, Ganetis et al. (2018) and Baxter and Schumacher (2017) were based on snowbands specifically. That choice favors the cold sector of the cyclone, so bands being farther south in our dataset relative to those two studies may reflect this difference.

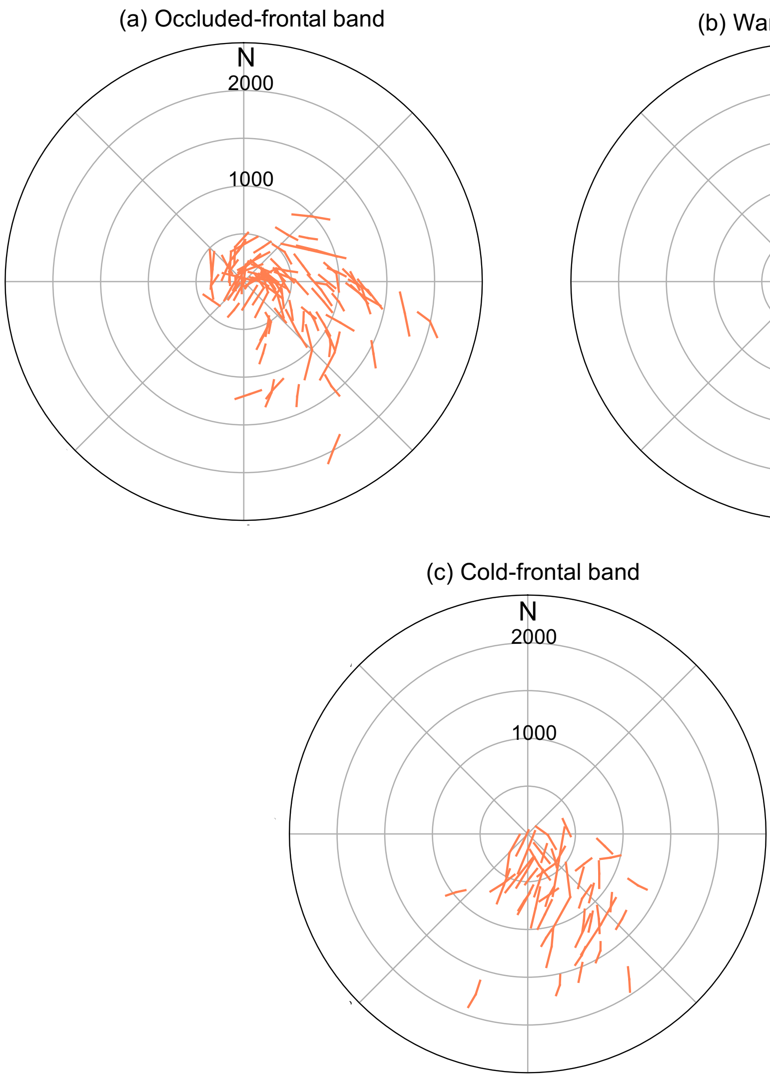

Figure 8. The distribution of (a) occluded-frontal bands, (b) warm-frontal bands, (c) cold-frontal bands relative to the low centers of their parent cyclones (origin). Red solid lines represent axes of precipitation bands at their formation times over the British Isles. Radial distance is in km.

The distance between a band and its parent cyclone center is measured from the midpoint of the band to the low center. The average distance is 647 km for occluded-frontal bands and 826 km for cold-frontal bands, with 76% and 67% being less than 1000 km away from their parent cyclones, respectively. In contrast, the longest average distance is 1026 km for warm-frontal bands, with 54% of warm-frontal bands being more than 1000 km away. However, Novak et al. (2004) showed that almost all their bands were within 1000 km of the cyclone center. Thus, bands in the northeast United States were closer to the cyclone than those in the British Isles. Two possible reasons can explain this difference. First, many cyclone centers with bands occurred near the east coast of the United States (Fig. 3 in Novak et al. 2004), but many cyclone centers occur far away from the British Isles (Fig. 2). Thus, bands are more likely to be farther away from low centers in the British Isles than for the east coast of the United States. Second, as extratropical cyclones expand in size at the end of the storm track (e.g., Oruba et al. 2013), bands near the British Isles find themselves in generally larger-scale cyclones than those of the eastern United States. Thus, bands in the British Isles will tend to be farther from the cyclone center than those in the eastern United States.

6. Synoptic composites of precipitation bands

To understand the typical synoptic environments that favor different types of precipitation bands, we create composite analyses from Met Office 5-min 1-km grid-spacing precipitation-rate mosaics (Kitchen and Illingworth 2011; Antonescu et al. 2013) and the European Centre for Medium-Range Weather Forecasts (ECMWF) ERA5 reanalyses (Hersbach et al. 2020). Based on this five-year climatology (Fig. 6), occluded-, warm-, and cold-frontal bands are most common over the British Isles. A common location for occluded-frontal (29%, or 27 out of 93 bands) and warm-frontal (31%, or 17 out of 54 bands) bands to form is near the west coast of Scotland. Of those bands, most are oriented northwest–southeast (19 occluded- and 14 warm-frontal bands) (Fig. 7). However, 44% (21 out of 48 bands) of cold-frontal bands form near southwest of Great Britain, with 90% (19 of those 21 bands) oriented southwest–northeast (Fig. 7). Therefore, we create three composites of common types of bands by location and orientation: northwest–southeast occluded-frontal bands west of Scotland, northwest–southeast warm-frontal bands west of Scotland, and southwest–northeast cold-frontal bands southwest of Great Britain. Similar patterns of precipitation between cases in each composite indicate a commonality in the characteristics of precipitation bands in cyclones of the British Isles and the processes that create them, both of which we develop further in the remainder of this section.

a. Data and method

Met Office 5-min, 1-km horizontal grid-spacing, precipitation-rate mosaics are available from 2004 until present over the British Isles from the Centre for Environmental Data Analysis. This radar dataset is the same as that used to create the Metcheck image archive discussed in section 2a. Composites of precipitation rate and their synoptic environments are constructed from ERA5 reanalyses, which are available from 1979 to present across the globe on 37 vertical pressure levels and 0.25° × 0.25° horizontal grid spacing (Hersbach et al. 2020). The time interval is one hour, longer than that of radar images from the Metcheck website; thus, we use the closest ERA5 reanalysis time before the formation time from the Metcheck website. In this study, we define t = 0 as the formation time of a band, and t = –12 h as 12 h before the formation of a band. The composite results are shown from t = –12 h to t = 0. MetPy version 1.3 is a Python package for calculating kinematic parameters and visualizing weather datasets (May et al. 2022). In this study, we use it to calculate 2D Petterssen (1936) frontogenesis and saturation equivalent potential vorticity (EPV), which assesses moist symmetric instability.

b. Radar-derived precipitation field

To emphasize the robustness of our composites, Fig. 9 illustrates where the heaviest precipitation falls for these three composite bands, using Met Office radar data and ERA5 reanalyses. For the occluded-frontal and warm-frontal composites, the banded regions with the heaviest precipitation rate are located west of Scotland and are oriented northwest–southeast (Figs. 9a,b,d,e). However, for cold-frontal bands, the banded region is located southwest of Great Britain and is oriented southwest–northeast (Figs. 9c,f). Apparently, the maximum precipitation rates in these regions are lower than 2 mm h^{-1} (i.e., our intensity criteria for banding) in three composites because averaging weakens the precipitation rates from the individual cases. Nonetheless, we define these regions as the composite positions of bands for different types. The observed composite bands and the ERA5 composite bands vary slightly in intensity, size, and location. For example, the maximum precipitation rates in the three observed composites are slightly heavier than those for the corresponding ERA5 composites. The banded regions are larger and located more northwest in the ERA5 composites than the observed composites for the occluded-frontal and warm-frontal bands. Despite some differences, the observed composite bands and the ERA5 composite bands are generally similar. Therefore, the consistent patterns of precipitation between observation and ERA5 reanalyses suggest that using ERA5 reanalyses is reasonable to analyze synoptic environments of observed composite bands.

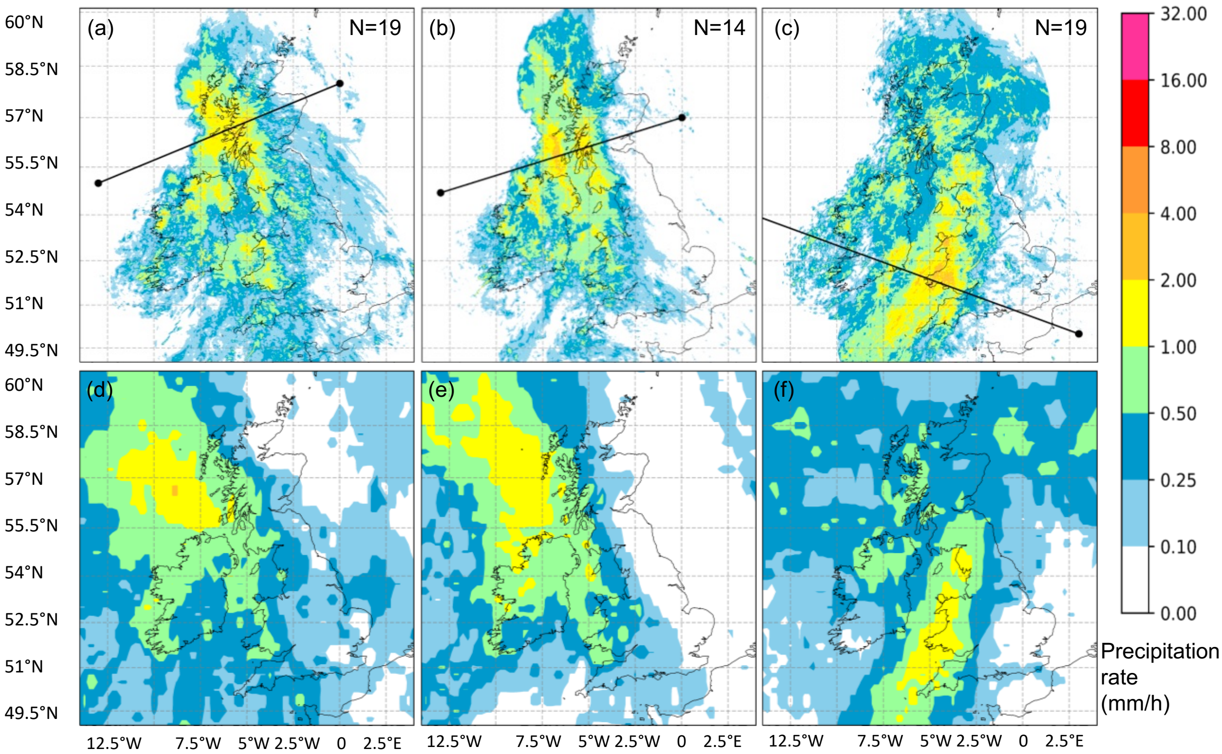

Figure 9. Mean precipitation rate (colored according to scale) of the number (N) of bands within each category at $t = 0$, using Met Office radar data: (a) northwest–southeast occluded-frontal bands west of Scotland, (b) northwest–southeast warm-frontal bands west of Scotland, and (c) southwest–northeast cold-frontal bands southwest of Great Britain. (d), (e), and (f) Same as in (a), (b), and (c) except using ERA5 reanalyses. Black lines in (a), (b), and (c) are cross-section orientations appearing in Figs. 13a,d, 13b,e, and 13c,f, respectively.

c. *Surface and upper-level fields*

This subsection investigates similarities and differences between the surface and upper-level environments that support the formation of the three types of precipitation bands created from the ERA5 composites. Figure 10 shows composite mean sea level pressure, 500-hPa geopotential heights, and 300-hPa wind speed at $t = –12$ h and $t = 0$. At $t = –12$ h, the surface cyclone occurs northwest of the British Isles in the three composites (Figs. 10a,c,e). Twelve hours later, all three composite surface cyclones move eastward, with the associated surface fronts approaching the mean locations of bands (Figs. 10b,d,f). The surface fronts in the occluded-frontal and warm-frontal composites are oriented northwest–southeast (Figs. 10a,b,c,d), whereas that in the cold-frontal composite is oriented northeast–southwest (Fig. 10e,f), all more-or-less meridionally oriented and consistent with the orientation of the composite bands. Surface fronts coincide with surface troughs, indicating the close relationship between the fronts and all types of composite bands.

At 500 hPa, a short-wave trough is upstream of the surface trough for the three types of composite bands at $t = –12$ h (Figs. 10a,c,e). By $t = 0$, for occluded-frontal and warm-frontal composites, the 500-hPa trough is nearly vertically stacked with the surface trough (Figs. 10b,d). However, for the cold-frontal composite, the 500-hPa trough remains behind the surface trough by $t = 0$ (Fig. 10f). The composite occluded and warm frontal bands are located underneath the 500-hPa ridge, where the winds veering with height lead to warm advection and ascent (Figs. 10b,d). The ridge amplitude in the warm-frontal composite is considerably stronger than that in the occluded-frontal composite due to weaker upper-level zonal winds and blocking. However, the composite cold-frontal band is near the inflection point between the trough and ridge, the favorable region for ascent due to the ω equation (Fig. 10f).

At 300 hPa, the strongest jet streak of up to 60 m s^{-1} in the occluded-frontal composite is behind the 500-hPa trough at $t = –12$ h and at $t = 0$ (Figs. 10a,b). A shorter jet maximum of 55 m s^{-1} is east of the 500-hPa trough at $t = –12$ h, which weakens and moves to the base of the trough by $t = 0$ (Figs. 10a,b). The composite occluded-frontal band is in the left-exit region of the 300-hPa jet steak at $t = 0$ (Fig. 10b), a favorable location for synoptic-scale ascent. In the warm-frontal composite, 300-hPa jet streaks are more distant from the surface low than other two composites (Figs. 10c,d). At t = 0, the jet streaks are about 500 km upstream and downstream of the band, suggesting little opportunity for jet coupling. In the cold-frontal composite, one jet streak is in the base of the 500-hPa trough and the other one is downstream of the trough at t = –12 h (Fig. 10e). Both jet streaks move eastward by t = 0, with the band found underneath the right-entrance region of the easternmost jet streak (Fig. 10f), also a favorable location for synoptic-scale ascent.

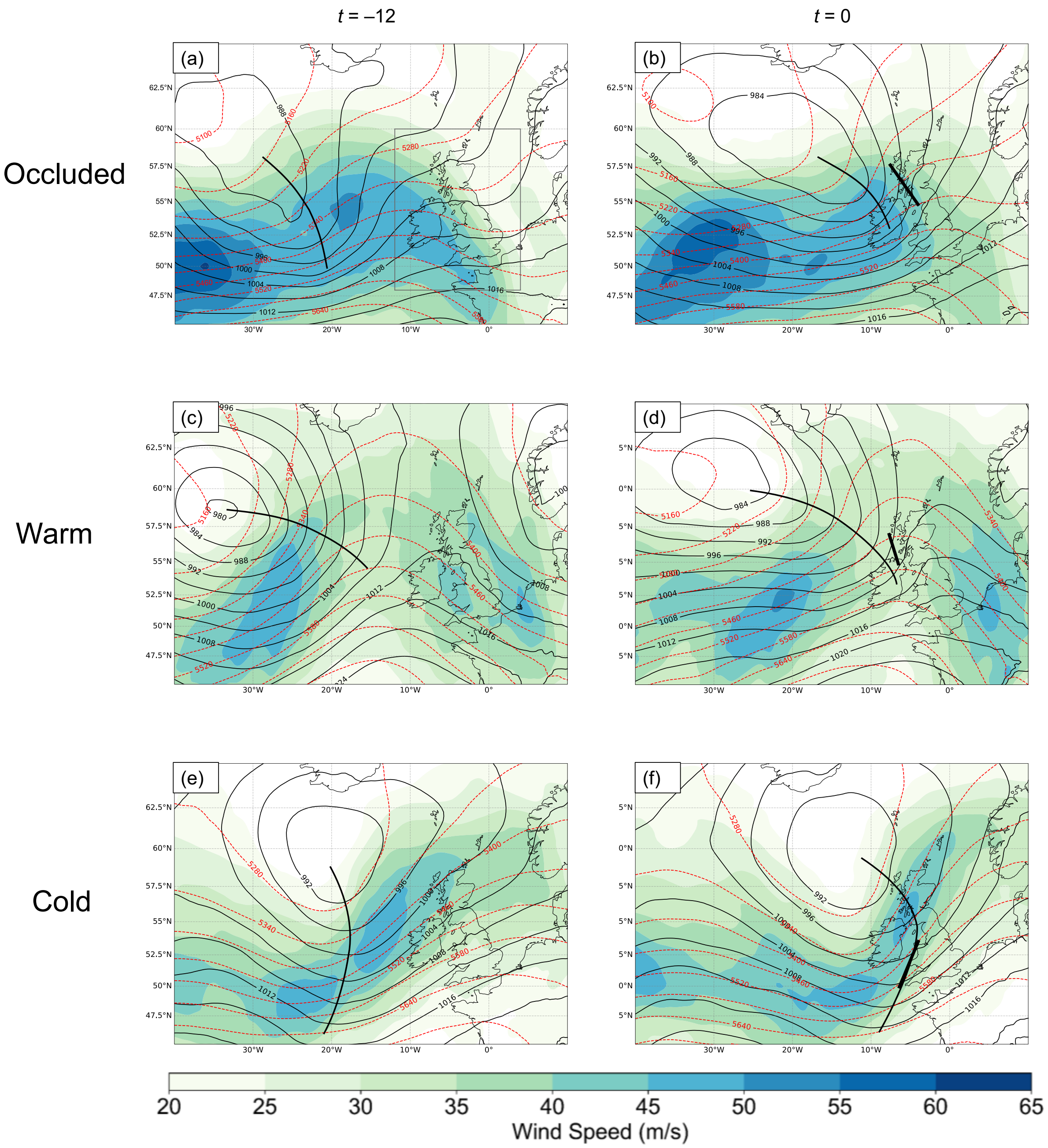

Figure 10. Mean sea level pressure (solid, every 4 hPa), 500-hPa geopotential heights (dashed,

every 60 m), and 300-hPa wind speeds (colored according to scale, starting at 20 m s^{-1}) for (a) northwest–southeast occluded-frontal bands west of Scotland, (c) northwest–southeast warm-frontal bands west of Scotland, and (e) southwest–northeast cold-frontal bands southwest of Great Britain at t = –12 h. (b), (d), and (f) Same as in (a), (c), and (e) except at t = 0. Black curves represent the mean front locations (fronts are identified by surface toughs, and potential temperature gradients). Black line segments in (b), (d), and (f) represent the mean band locations at their formation time. Gray boxes represent the radar domain described in section 2.

d. Low-level wind fields

This subsection reveals the relationship between the low-level wind and the three composite bands. Figure 11 shows 925-hPa wind at $t = -12$ h and $t = 0$. At $t = -12$ h, a 925-hPa jet is located southwest of the British Isles for each of the three composites (Figs. 11a,c,e). The composite maximum wind speeds are stronger in the occluded-frontal and warm-frontal composites (30 m s^{-1} and 25 m s^{-1}, respectively) than in the cold-frontal composite (21 m s^{-1}) (Figs. 11a,c,e). This result is associated with the weaker sea-level pressure gradient in the cold-frontal composite. Two reasons are responsible for the relatively weak sea-level pressure gradient in the cold-frontal composite compared to the other two composites. First, warm and occluded fronts need to be associated with a deep cyclone to produce a linear precipitation band over the British Isles, while cold fronts are more likely to create such bands even within relatively weak cyclones. Second is the larger variety of locations of individual cyclones (thereby more smearing out the pressure field in the cold-frontal composite). Twelve hours later, the low-level jet extends to the west coast of Scotland in the occluded-frontal and warm-frontal composites, and to the southwest coast of Great Britain in the cold-frontal composite (Figs. 11b,d,f). The composite wind speed weakens by about 5 m s^{-1} in the occluded-frontal and warm-frontal composites, but remains nearly unchanged in the cold-frontal composite, narrowing in all three composites (Figs. 11b,d,f). The positions where the low-level jets intersect the frontal zones are coincident with the mean band positions (Figs. 11b,d,f). Particularly, the width of the jet maximum of about 300 km matches the composite length of composite occluded-frontal and warm-frontal bands. In the following, we will explain the relationship between low-level jets and composite bands.

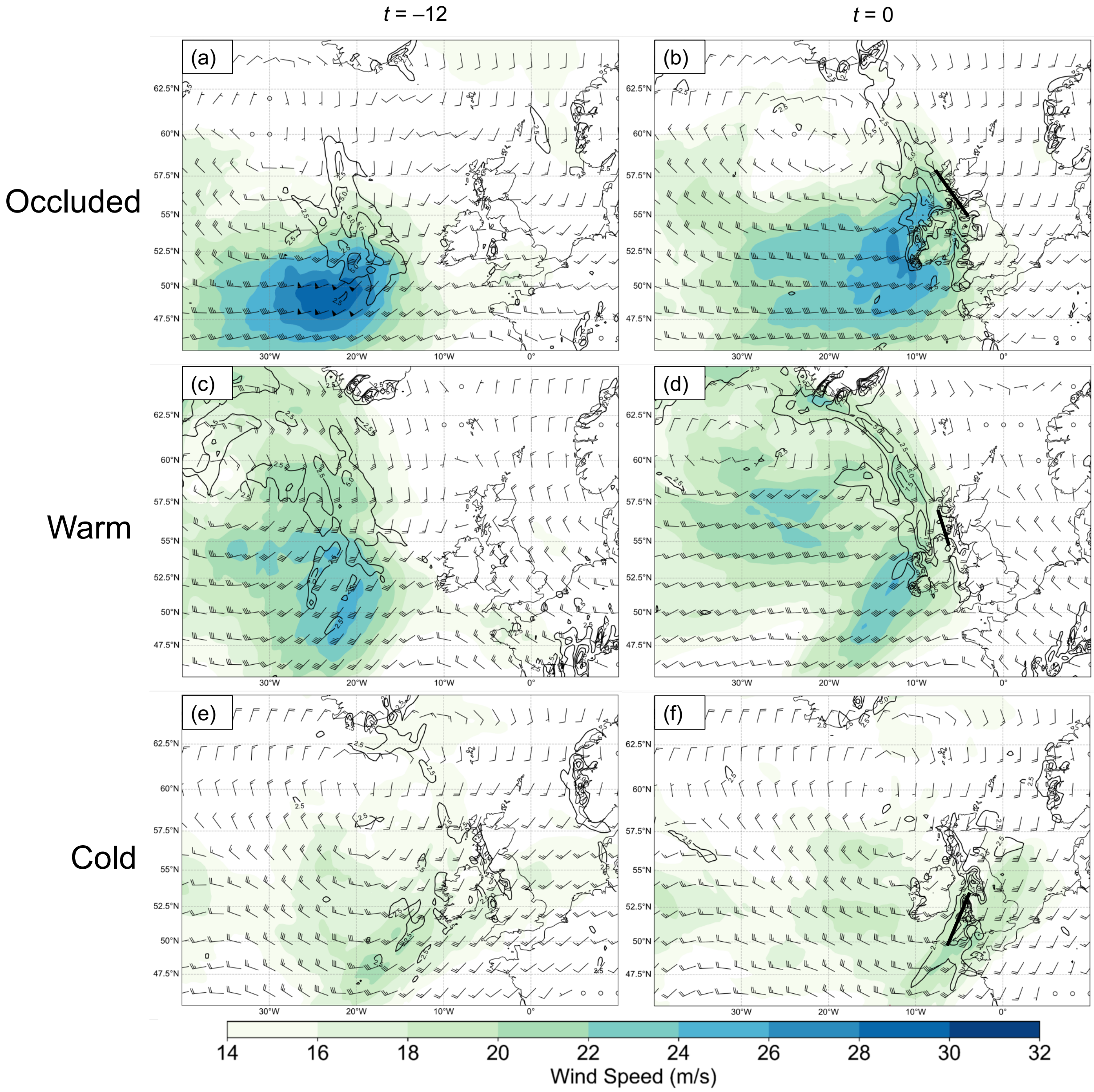

Figure 11. 925-hPa wind speed (colored according to scale, starting at 14 m s^{-1}), wind vector (pennant, full barb, and half-barb denote 25, 5, 2.5 m s^{-1}, respectively; circles represent calm winds), and 800-hPa vertical velocity (solid, every 2.5 m s^{-1}) for (a) northwest–southeast occluded-frontal bands west of Scotland, (c) northwest–southeast warm-frontal bands west of Scotland, and (e) southwest–northeast cold-frontal bands southwest of Great Britain at *t* = –12 h. (b), (d), and (f) Same as in (a), (c), and (e) except at *t* = 0. Black line segments in (b), (d), and (f) represent the mean band locations at their formation time.

Next, the likely dynamical and thermodynamical linkages between the low-level jet and the composite precipitation band are shown in the following figures (Figs. 11 and 12). First, comparing the 900-hPa jet with the horizontal distribution of 800-hPa ascent can illustrate the dynamic linkages (Fig. 11). In all three cases, the low-level ascent is weak near the low-level jet at $t = -12$ h. At $t = 0$, as the low-level jet extends to the northeast, the ascent increases along the front. However, the maximum low-level ascent regions occur in the part of front with the low-level jet (behind the composite occluded-frontal and warm-frontal bands, and along the composite cold-frontal band), not the whole front. The scale of the maximum low-level ascent region is similar to the scale of band. Therefore, the low-level jet is associated with the location of strong ascent for precipitation bands.

Second, to illustrate the thermodynamic linkage, the 925-hPa potential temperature and specific humidity are shown in Fig. 12. At $t = -12$ h, regions with the highest specific humidity of around 7 g kg^{-1} are coincident with those with the highest potential temperature (Figs. 12a,c,e). The warm moist tongue extends northeastward along the edge of the 925-hPa jet and approaches the coast over time (Figs. 12b,d,f). This structure in the composites is similar to an atmospheric river, which transports warm moist air in a narrow low-level jet ahead of the cold front (e.g., Ralph et al. 2004; Gimeno et al. 2016; Ralph et al. 2018). Although the thermodynamic structures in the occluded-frontal and warm-frontal composites are similar, the thermal ridge is broader and weaker for the composite occluded-frontal band than the composite warm-frontal band. The reason is that, in the occluded-frontal composite, a broader region of baroclinicity (i.e., temperature gradient) extending southwestward represents a region over which the individual trailing cold fronts are less likely to occur in a specific position (Fig. 12b). The highest horizontal moisture transport vectors in the occluded-frontal and warm-frontal composites are from southwest to northeast behind the front, normal to the potential temperature and specific humidity contours (Figs. 12a,b,c,d). In contrast, the highest horizontal moisture transport vectors in the cold-frontal composite are nearly parallel to the potential temperature and specific humidity contours ahead of the front (Figs. 12e,f). These horizontal moisture transport vectors have a component of motion forward relative to the cold front (Fig. 12f), consistent with the conceptual model of the warm conveyor belt with forward-sloping ascent, common in the United Kingdom (e.g., Browning 1986).

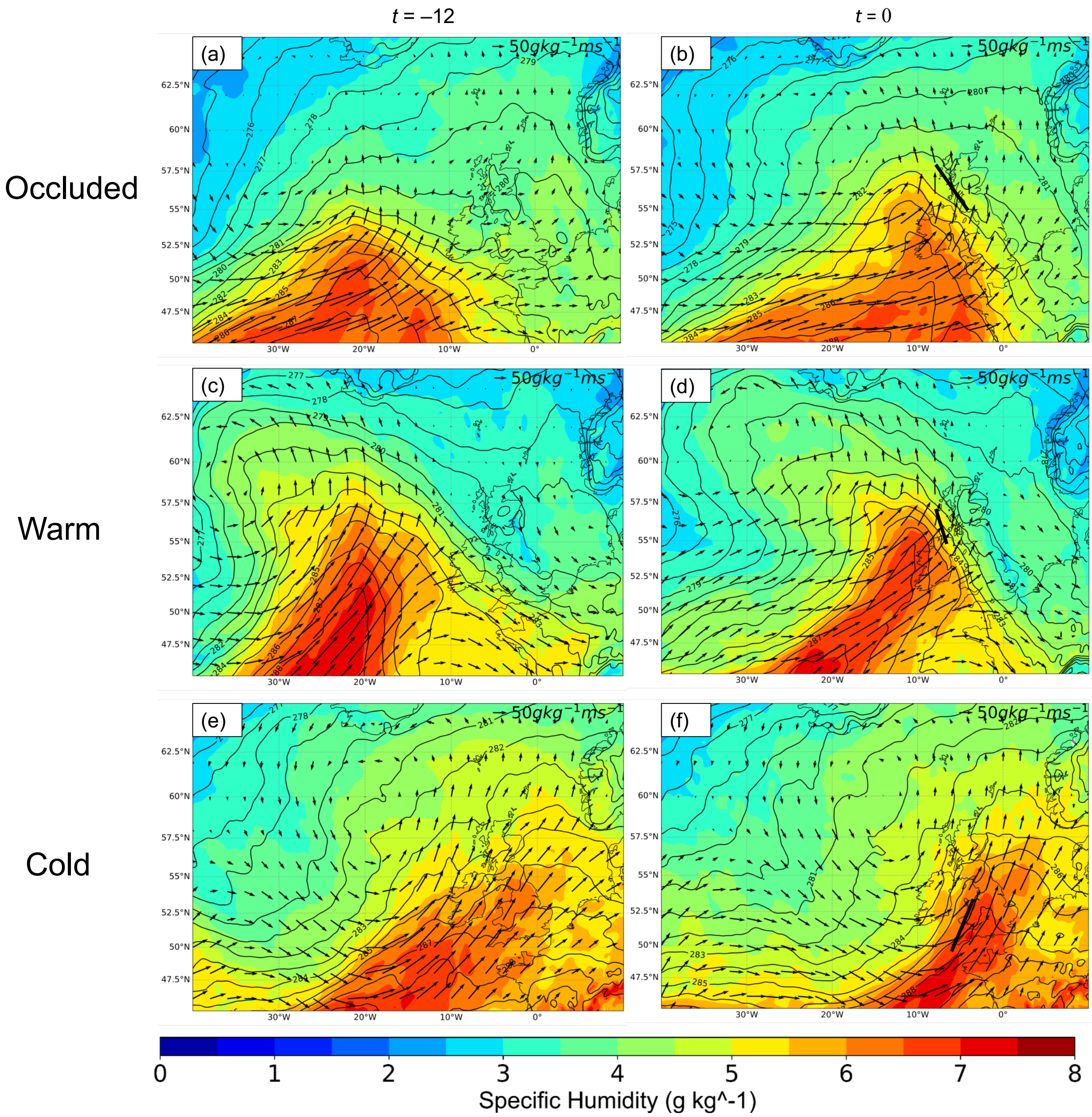

Figure 12. 925-hPa specific humidity (g kg^{-1}, colored according to scale), potential temperature (θ, solid, every 1 K), and horizontal moisture transport vectors (g kg^{-1} m s^{-1}, arrows) for (a) northwest–southeast occluded-frontal bands west of Scotland, (c) northwest–southeast warm-frontal bands west of Scotland, and (e) southwest–northeast cold-frontal bands southwest of Great Britain at $t = -12$ h. (b), (d), and (f) Same as in (a), (c), and (e) except at $t = 0$. Black line segments in (b), (d), and (f) represent the mean band locations at their formation time.

e. Vertical cross sections of instability and frontogenesis

To further understand the vertical structures of the three different composite bands, Fig. 13 shows composite cross-sectional analyses. These cross sections illustrate similar structures to fronts in conceptual models and in previously published composite analyses of banded precipitation (e.g., Novak et al. 2004; Baxter and Schumacher 2017). Specifically, isotherms tilt rearward in the cold-frontal composite (Fig. 13e), but forward in the warm-frontal composite (Fig. 13c). However, isotherms in the occluded-frontal composite (Fig. 13a) are concave in the middle troposphere (500–700 hPa), indicating the likely elevated cold-frontal zone of the occluded front. The warm sector is narrower and elevated in the occluded-frontal composite, which is not present in the warm-frontal composite where the warm sector is much wider (Figs. 13a,c), consistent with common conceptual models of fronts. The horizontal wind shift with height is weaker and is always southwesterly with height in the cold-frontal composite compared to the others. However, in the occluded-frontal composite, the winds are southerly at low levels shifting to southwesterly with height, and in the warm-frontal composite the wind shifts to westerly with height.

The region of frontogenesis exceeding 0.4 K (100 km 3 h)$^{-1}$ slopes eastward in the occluded-frontal and the warm-frontal composites (Fig. 13a,c), but slopes westward in the cold-frontal composite (Fig. 13e). The slope of frontogenesis in occluded-frontal and warm-frontal composites is shallower than that in the cold-frontal composite (cf. Figs. 13a,c and Fig. 13e). The ascent maximum is 14 cm s^{-1} at 600 hPa in the occluded-frontal composites and 9 cm s^{-1} at 800 hPa in the warm-frontal composite (Figs. 13a,c). The cold-frontal band is associated with two separate ascent maxima of 8 cm s^{-1} at 850 and 600 hPa (Fig. 13e). The maximum ascent occurs on the warm side of the frontal region (Figs. 13a,c,e), consistent with the direct circulation induced by frontogenesis based on Sawyer–Eliassen equation (Sawyer 1956; Eliassen 1962; Emanuel 1985; Xu 1992). The mean position of the occluded-frontal band and warm-frontal band is found ahead of the maximum ascent (Figs. 13a,c), because the warm moist air rises slantwise up before it condenses and forms clouds and precipitation. However, the mean position of cold-frontal band is directly under the maximum ascent (Fig. 13e), because the ascent is right along the leading edge of the front.

In all three composites, a region of negative EPV with the saturation equivalent potential temperature (θ_{es}) folding below 900 hPa shows that the atmosphere is conditionally unstable in the oceanic boundary layer (Figs. 13b,d,f). Above the boundary layer, the air becomes symmetrically stable in the occluded-frontal and warm-frontal composites, if it is lifted to the region with positive EPV and high relatively humidity (RH > 70%) (Figs. 13b,d). However, the atmosphere in the cold-frontal composite is less symmetrically stable than that in the other two composites. Because the θ_{es} lapse rate is near zero, small EPV (i.e., EPV < 0.25 PVU) with high RH suggests small moist symmetric stability (Fig. 13e). Therefore, the frontogenesis with small moist symmetric stability in a deep layer of 900–600 hPa directly above the mean band position is a potential mechanism to provide forcing for the cold-frontal band (e.g., Emanuel 1985; Nicosia and Grumm 1999; Novak et al. 2004).

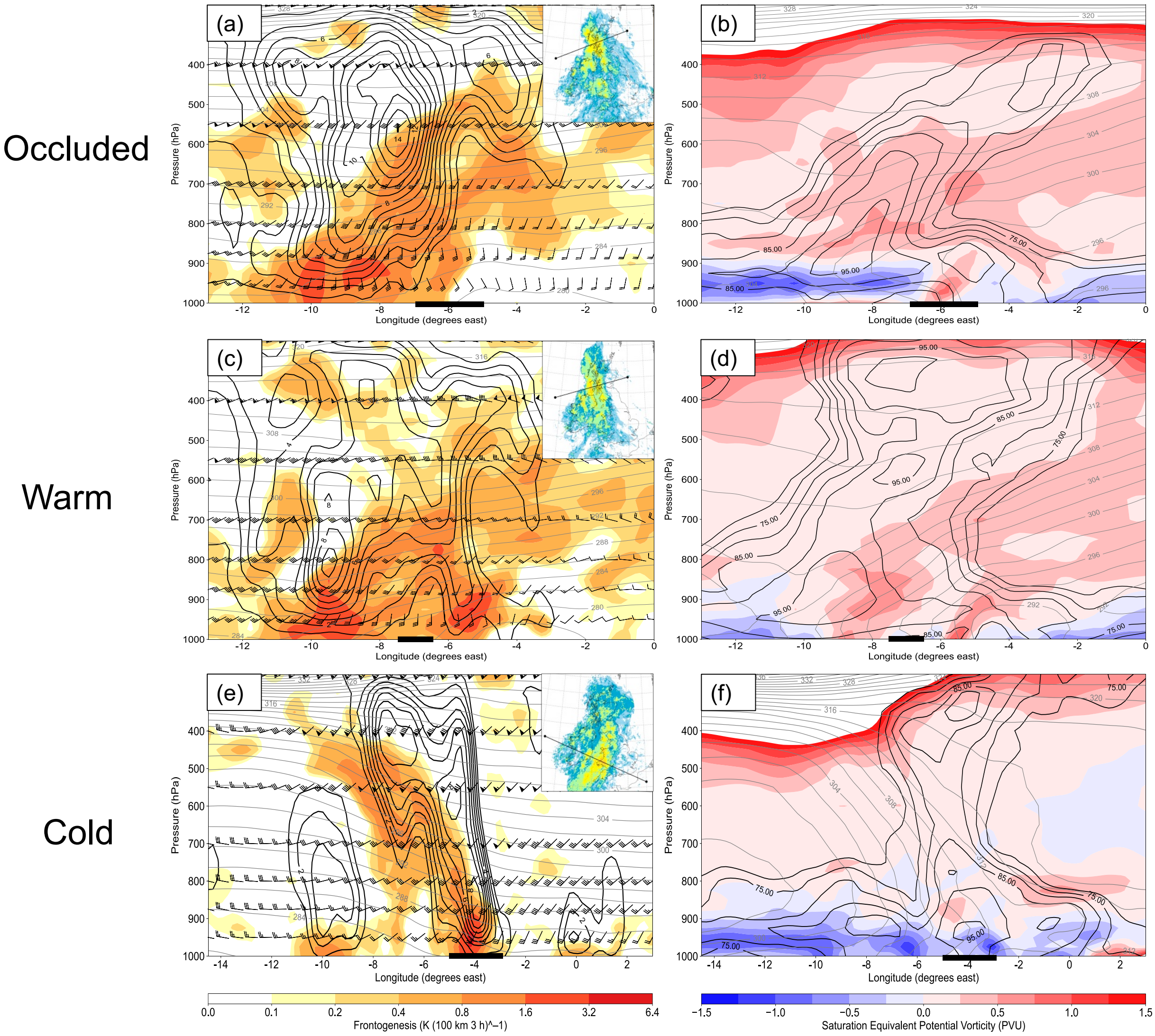

Figure 13. Cross section through the composite occluded-frontal band (black bar along *x* axis) at $t = 0$: (a) Petterssen frontogenesis [shaded positive values according to scale in units of K (100 km 3 h)$^{-1}$], ascent (black solid lines every 1 cm s^{-1}), potential temperature (θ, gray solid lines every 2 K), and horizontal wind vector (pennant, full barb, and half-barb denote 25, 5, 2.5 m s^{-1}, respectively). (b) Saturation equivalent potential vorticity, calculated using the full wind (shaded, every 0.25 PVU), relative humidity (black solid lines every 5%, starting from 70%), and saturation equivalent potential temperature (θ_{es}, gray solid lines every 2 K); (c) and (d) Same as in (a), (b) except for the warm-frontal band. (e) and (f) Same as in (a), (b) except for the cold-frontal band. Inset for Fig. 9 to show cross section orientations.

7. Conclusion

Although other studies from the northeastern and central United States have constructed climatologies and synoptic composites of precipitation bands associated with extratropical cyclones (i.e., Novak et al. 2004; Baxter et al. 2017), such a study has not been performed for the British Isles. In this article, DWD surface maps and Met Office radar data were used to identify 249 precipitation bands and their 167 parent extratropical cyclones over the British Isles from April 2017 to March 2022. Bands formed commonly west of Scotland in winter and spring, and west of Ireland in summer and autumn, mostly with a meridional orientation as opposed to a more zonal orientation, suggesting that the fronts and bands were being stretched meridionally, as would be occurring at the jet-exit region of the North Atlantic storm track. Also, more bands formed over water near the coasts than over land (151 versus 98). The average length of bands at their maximum length was about 460 km, longer than that at their formation time (290 km), indicating an increasing length with the development of bands. Most bands were generally short-lived, with bands lasting 2–3 h most common, with few bands lasting longer than 10 h.

Bands were classified into six categories: occluded-frontal bands, warm-frontal bands, cold-frontal bands, postfrontal bands, warm-sector bands, and other bands. Occluded-frontal bands observed are the most frequent (19 yr^{-1}), followed by warm-frontal bands (11 yr^{-1}), cold-frontal bands (10 yr^{-1}), postfrontal bands (4 yr^{-1}), and warm-sector bands (4 yr^{-1}). However, the mean durations did not vary substantially for the six types of bands, with a range from shortest (warm-frontal bands at 3.8 h) to the longest (cold-frontal bands at 4.8 h). Among the six types of bands, occluded-frontal and warm-frontal bands were most common west of Scotland, were east relative to their parent cyclones, and were oriented northwest–southeast at the formation time. In contrast, most cold-frontal bands formed near the southwest coastline of Great Britain, were south relative to their cyclones, and were oriented south-southwest–north-northeast.

To study synoptic environments for various types of bands, we constructed three composites: northwest–southeast occluded-frontal bands west of Scotland, northwest–southeast warm-frontal bands west of Scotland, and southwest–northeast cold-frontal bands southwest of Great Britain. Conceptual models of these three types of bands summarize their key composite features in Fig. 14. For the composite occluded-frontal and warm-frontal bands, a northwest–southeast surface trough is collocated with the front extending from a cyclone located to the northwest of the British Isles and nearly vertically stacked with a 500-hPa trough (Figs. 14a,b). However, for the composite cold-frontal band, a northeast–southwest surface cold front extends from a cyclone located to the northwest of the British Isles and ahead of a 500-hPa trough (Fig. 14c). The composite occluded-frontal band occurs in the left-exit region of a 300-hPa jet streak (Fig. 14a), and the composite cold-frontal band occurs in the right-entrance region of the easternmost jet streak (Fig. 14c), but the composite warm-frontal band lies under a local wind-speed minimum (Fig. 14b). The low-level jet is associated with moisture transport and ascent. In particular, the scale of the low-level jet is associated with the length of composite occluded-frontal and warm-frontal bands (Figs. 14a,b), indicating possible utility in predicting where and how long such bands are most likely to form, in a manner analogous to an atmospheric river. Cross sections through these three bands are similar to those previously published elsewhere (e.g., Novak et al. 2004; Baxter and Schumacher 2017).

Compared to precipitation bands in the northeastern United States (i.e., Novak et al. 2004) and snowbands in the central United States (i.e., Baxter and Schumacher 2017) that tend to form to the north or northeast of the low center with more zonal orientations, precipitation bands in the British Isles tend to form east and southeast of the low centers with more meridional orientation. This difference is likely due to the U.S. radar network being west of the cyclones and cyclones being in the jet-entrance region of the North Atlantic storm track where fronts and precipitation bands would be zonally stretched versus British radar network being east of the cyclones and cyclones being in the jet-exit region where fronts and precipitation would be meridionally stretched. Precipitation bands in all three composite locations over the British Isles tend to have similar durations and lengths, although precipitation bands in the British Isles tend to occur farther away from the low center than those in the United States.

A five-year climatology of banded precipitation provides a dataset of cases and further insight into the processes that create banded precipitation. Such a dataset can provide a check on the output from model forecasts to verify if the bulk characteristics of modelled precipitation bands resemble those that are observed. Such a dataset can also make forecasters aware of when and where bands form most commonly (both geographically and within the cyclones themselves) and help them to further understand physical mechanisms of different band types using the frontal-type classification in operational settings. These results also help explain that precipitation does not have uniform intensity all along the front, but instead is focused on the region where the low-level jet approaches the frontal zone and undergoes ascent. These results also show that precipitation bands often do not last for more than a few hours. Finally, these results show that, although there are a number of similarities between the results of this study in the British Isles and those elsewhere (particularly the United States), the characteristics of precipitation bands can have considerable geographical variability, suggesting caution when applying the results of precipitation band climatologies from one area to another around the globe and the need to document banded precipitation in other regions around the globe.

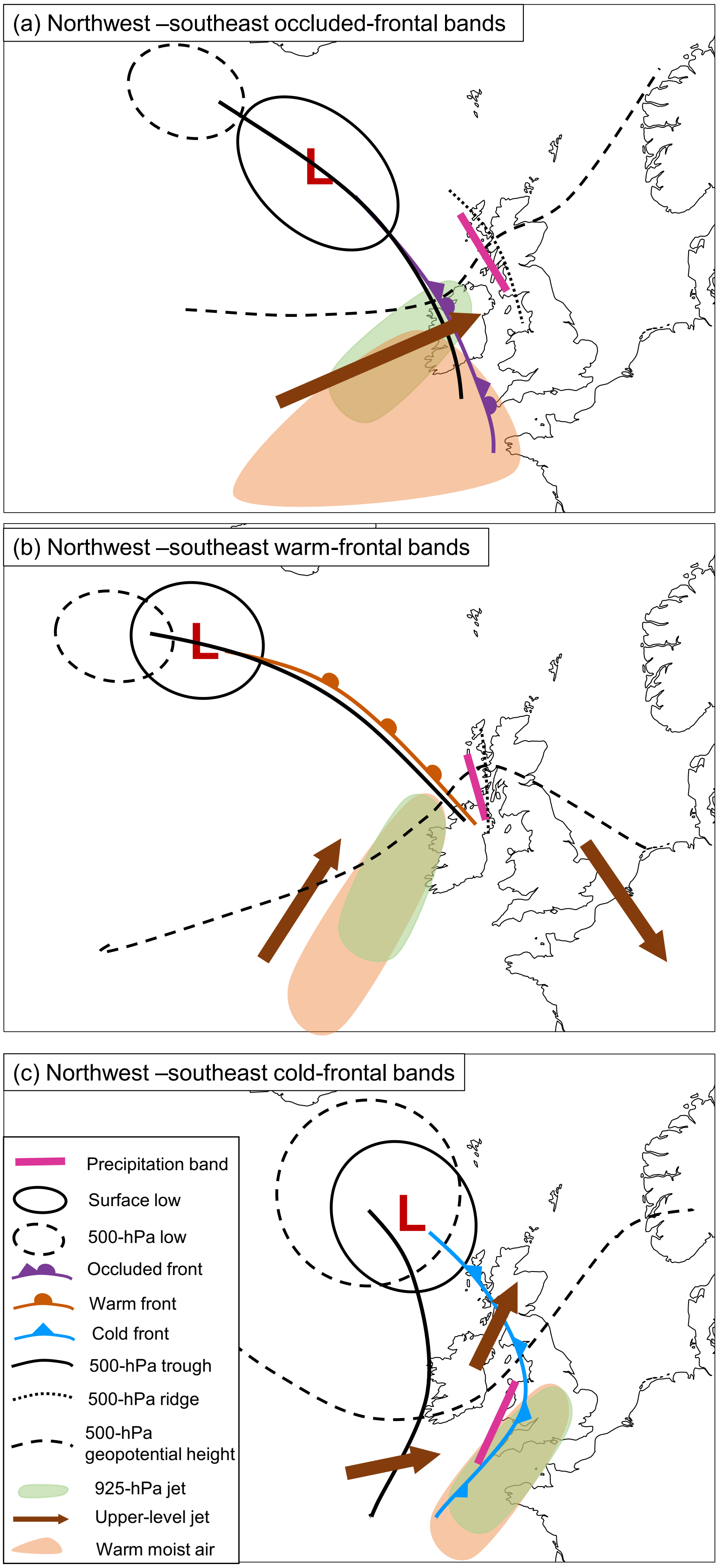
(a) Northwest –southeast occluded-frontal bands
L
(b) Northwest –southeast warm-frontal bands
L
(c) Northwest –southeast cold-frontal bands
L
Precipitation band
Surface low
500-hPa low
Occluded front
Warm front
Cold front
500-hPa trough
500-hPa ridge
500-hPa geopotential height
925-hPa jet
Upper-level jet
Warm moist air

725

Figure 14. Conceptual models of the salient features in synoptic environments associated with (a) a northwest–southeast occluded-frontal band west of Scotland, (b) northwest–southeast warm-frontal band west of Scotland, and (c) southwest–northeast cold-frontal band southwest of Great Britain. Features are composite band (pink line), surface cyclone (black circle), 500-hPa low (black dashed circle), surface front (purple line is occluded front, red line is warm front, blue line is cold front), 500-hPa trough axis (black line), 500-hPa ridge axis (dotted line), 500-hPa geopotential height (dashed line), 925-hPa warm moist air (red fill), 925-hPa jet (green fill), and 300-hPa jet (brown arrow).

Acknowledgements. This article is a contribution to Zhang's Ph.D. dissertation. Partial funding for Schultz was provided to the University of Manchester by the Natural Environment Research Council through Grants NE/N003918/1 and NE/W000997/1. We thank Chief Editor Gary Lackmann and the anonymous peer reviewers who provided comments to help improve this article.

Data Availability Statement. The DWD surface maps are freely available through the following archive (http://www1.wetter3.de/). Radar imagery for the band identification in section 2 were purchased through access to the Metcheck radar-imagery archive (https://www.metcheck.com/WEATHER/archived_radar.asp). ERA5 data were downloaded from the Copernicus Climate Data Store (https://cds.climate.copernicus.eu/cdsapp#!/dataset/reanalysis-era5-pressure-levels). Met Office digital radar data for Figs. 1 and 11 were obtained from the Centre for Environmental Data Analysis (https://catalogue.ceda.ac.uk/uuid/27dd6ffba67f667a18c62de5c3456350).

References

Antonescu, B., G. Vaughan, and D. M. Schultz, 2013: A five-year radar-based climatology of tropopause folds and deep convection over Wales, United Kingdom. *Mon. Wea. Rev.*, **141,** 1693–1707.

Baxter, M. A., and P. N. Schumacher, 2017: Distribution of single-banded snowfall in central U.S. cyclones. *Wea. Forecasting*, **32,** 533–554.

Bergeron, T., 1937: On the physics of fronts. *Bull. Amer. Meteor. Soc.*, **18,** 265–275.

Browning, K. A., 1986: Conceptual models of precipitation systems. *Wea. Forecasting*, **1,** 23–41.

Browning, K. A., and C. W. Pardoe, 1973: Structure of low-level jet streams ahead of mid-latitude cold fronts. *Quart. J. Roy. Meteor. Soc.*, **99,** 619–638.

Colle, B. A., C. F. Mass, and B. F. Smull, 1999: An observational and numerical study of a cold front interacting with the Olympic Mountains during COAST IOP 5. *Mon. Wea. Rev.*, **127,** 1310–1334.

Colle, B. A., B. F. Smull, and M.-J. Yang, 2002: Numerical simulations of a landfalling cold front observed during COAST: Rapid evolution and responsible mechanisms. *Mon. Wea. Rev.*, **130,** 1945–1966.

Dacre, H. F., and S. L. Gray, 2009: The spatial distribution and evolution characteristics of North Atlantic cyclones. *Mon. Wea. Rev.*, **137,** 99–115.

Doswell, C. A., III, 1991: Comments on “Mesoscale convective patterns of the southern High Plains.”. *Bull. Amer. Meteor. Soc.*, **72,** 389–390.

Eliassen, A., 1962: On the vertical circulation in frontal zones. *Geofys. Publ.*, **24,** 147–160.

Emanuel, K. A., 1985: Frontal circulations in the presence of small moist symmetric stability. *J. Atmos. Sci.*, **42,** 1062–1071.

Fairman, J. G., Jr., D. M. Schultz, D. J. Kirshbaum, S. L. Gray, and A. I. Barrett, 2016: Climatology of banded precipitation over the contiguous United States. *Mon. Wea. Rev.*, **144,** 4553–4568.

——, 2017: Climatology of size, shape, and intensity of precipitation features over Great Britain and Ireland. *J. Hydrometeor.*, **18,** 1595–1615.

Ganetis, S. A., B. A. Colle, S. E. Yuter, and N. P. Hoban, 2018: Environmental conditions associated with observed snowband structures within northeast U.S. winter storms. *Mon. Wea. Rev.*, **146,** 3675–3690.

Gimeno, L., and Coauthors, 2016: Major mechanisms of atmospheric moisture transport and their role in extreme precipitation events. *Annu. Rev. Environ. Resour.* , **41,** 117–141.

Gulev, S. K., O. Zolina, and S. Grigoriev, 2001: Extratropical cyclone variability in the Northern Hemisphere winter from the NCEP/NCAR reanalysis data. *Climate. Dyn.*, **17,** 795–809.

Hawcroft, M. K., L. C. Shaffrey, K. I. Hodges, and H. F. Dacre, 2012: How much Northern Hemisphere precipitation is associated with extratropical cyclones? *Geophys. Res. Lett.*, **39,**

L24809.
Hersbach, H., and Coauthors, 2020: The ERA5 global reanalysis. *Quart. J. Roy. Meteor. Soc.*, **146,** 1999-2049.
Hitchcock, S. M., T. P. Lane, R. A. Warren, and J. S. Soderholm, 2021: Linear rainfall features and their association with rainfall extremes near Melbourne, Australia. *Mon. Wea. Rev.*, **149,** 3401–3417.
Hobbs, P. V., 1978: Organization and structure of clouds and precipitation on the mesoscale and microscale in cyclonic storms. *Rev. Geophys. Space Phys.*, **16,** 741–755.
Houze, R. A., Jr., 2014: *Cloud Dynamics*. 2nd ed., Elsevier, 496 pp.
Houze, R. A., Jr., and P. V. Hobbs, 1982: Organization and structure of precipitating cloud systems. *Adv. Geophys.*, **24**, 225–315.
Houze, R. A., Jr., P. V. Hobbs, K. R. Biswas, and W. M. Davis, 1976: Mesoscale rainbands in extratropical cyclones. *Mon. Wea. Rev.*, **104,** 868–878.
Kawashima, M., 2016: The role of vertically propagating gravity waves forced by melting-induced cooling in the formation and evolution of wide cold-frontal rainbands. *J. Atmos. Sci.*, **73,** 2803–2836.
Kitchen, M., and A. J. Illingworth, 2011: The UK weather radar network – Past, present and future. *Weather*, **66,** 291–297.
Lackmann, G. M., 2002: Cold-frontal potential vorticity maxima, the low-level jet, and moisture transport in extratropical cyclones. *Mon. Wea. Rev.*, **130,** 59–74.
Matejka, T. J., R. A. Houze Jr., and P. V. Hobbs, 1980: Microphysics and dynamics of clouds associated with mesoscale rainbands in extratropical cyclones. *Quart. J. Roy. Meteor. Soc.*, **106,** 29–56.
May, R. M., and Coauthors, 2022: MetPy: A meteorological Python library for data analysis and visualization. *Bull. Amer. Meteor. Soc.*, **103,** 2273–2284.
Moore, J. T., C. E. Graves, S. Ng, and J. L. Smith, 2005: A process-oriented methodology toward understanding the organization of an extensive mesoscale snowband: A diagnostic case study of 4–5 December 1999. *Wea. Forecasting*, **20,** 35–50.
Muir, L. C., and M. J. Reeder, 2010: Idealized modelling of landfalling cold fronts. *Quart. J. Roy. Meteor. Soc.*, **136,** 2147–2161.

Nicosia, D. J., and R. H. Grumm, 1999: Mesoscale band formation in three major northeastern United States snowstorms. *Wea. Forecasting*, **14,** 346–368.

Ninomiya, K., and T. Akiyama, 1974: Band structure of mesoscale echo clusters associated with low-level jet stream. *J. Meteor. Soc. Japan*, **52,** 300–313.

Novak, D. R., B. A. Colle, and S. E. Yuter, 2008: High-resolution observations and model simulations of the life cycle of an intense mesoscale snowband over the northeastern United States. *Mon. Wea. Rev.*, **136,** 1433–1456.

Novak, D. R., B. A. Colle, and A. R. Aiyyer, 2010: Evolution of mesoscale precipitation band environments within the comma head of northeast U.S. cyclones. *Mon. Wea. Rev.*, **138,** 2354–2374.

Novak, D. R., L. F. Bosart, D. Keyser, and J. S. Waldstreicher, 2004: An observational study of cold season–banded precipitation in northeast US cyclones. *Wea. Forecasting*, **19,** 993–1010.

Oruba, L., G. Lapeyre, and G. Rivière, 2013: On the poleward motion of midlatitude cyclones in a baroclinic meandering jet. *J. Atmos. Sci.*, **70,** 2629–2649.

Parsons, D. B., and P. V. Hobbs, 1983: The mesoscale and microscale structure and organization of clouds and precipitation in midlatitude cyclones. VII: Formation, development, interaction and dissipation of rainbands. *J. Atmos. Sci.*, **40,** 559–579.

Ralph, F. M., P. J. Neiman, and G. A. Wick, 2004: Satellite and CALJET aircraft observations of atmospheric rivers over the eastern North Pacific Ocean during the winter of 1997/98. *Mon. Wea. Rev.*, **132,** 1721–1745.

Ralph, F. M., M. D. Dettinger, M. M. Cairns, T. J. Galarneau, and J. Eylander, 2018: Defining “atmospheric river”: How the *Glossary of Meteorology* helped resolve a debate. *Bull. Amer. Meteor. Soc.*, **99,** 837–839.

Sanders, F., 1986: Frontogenesis and symmetric stability in a major New England snowstorm. *Mon. Wea. Rev.*, **114,** 1847–1862.

Sansom, H. W., 1951: A study of cold fronts over the British Isles. *Quart. J. Roy. Meteor. Soc.*, **77,** 96–120.

Sawyer, J. S., 1956: The vertical circulation at meteorological fronts and its relation to frontogenesis. *Proceedings of the Royal Society of London. Series A. Mathematical and Physical Sciences*, **234,** 346–362.

Schultz, D. M., and P. N. Schumacher, 1999: The use and misuse of conditional symmetric instability. *Mont. Wea. Rev.*, **127,** 2709–2732.

Schultz, D. M., and F. Zhang, 2007: Baroclinic development within zonally-varying flows. *Quart. J. Roy. Meteor. Soc.*, **133,** 1101–1112.

Schultz, D. M., D. Keyser, and L. F. Bosart, 1998: The effect of large-scale flow on low-level frontal structure and evolution in midlatitude cyclones. *Mon. Wea. Rev.*, **126,** 1767–1791.

Thorpe, A., and K. Emanuel, 1985: Frontogenesis in the presence of small stability to slantwise convection. *J. Atmos. Sci.*, **42,** 1809–1824.

Xu, Q., 1989: Extended Sawyer–Eliassen equation for frontal circulations in the presence of small viscous moist symmetric stability. *J. Atmos. Sci.*, **46,** 2671–2683.

——, 1992: Formation and evolution of frontal rainbands and geostrophic potential vorticity anomalies. *J. Atmos. Sci.*, **49,** 629–648.

Yu, C. K., and B. F. Smull, 2000: Airborne Doppler observations of a landfalling cold front upstream of steep coastal orography. *Mon. Wea. Rev.*, **128,** 1577–1603.